Available online at www.sciencedirect.com

ScienceDirect

International Journal of Solids and Structures 44 (2007) 7816–7840

INTERNATIONAL JOURNAL OF SOLIDS AND STRUCTURES

www.elsevier.com/locate/ijsolstr

Mixed-mode fracture analysis of orthotropic functionally graded materials under mechanical and thermal loads

Serkan Dag [a,*], Bora Yildirim [b], Duygu Sarikaya [a]

[a] *Department of Mechanical Engineering, Middle East Technical University, Ankara 06531, Turkey*
[b] *Department of Mechanical Engineering, Hacettepe University, Ankara 06800, Turkey*

Received 27 December 2006; received in revised form 20 March 2007
Available online 23 May 2007

Abstract

Mixed-mode fracture problems of orthotropic functionally graded materials (FGMs) are examined under mechanical and thermal loading conditions. In the case of mechanical loading, an embedded crack in an orthotropic FGM layer is considered. The crack is assumed to be loaded by arbitrary normal and shear tractions that are applied to its surfaces. An analytical solution based on the singular integral equations and a numerical approach based on the enriched finite elements are developed to evaluate the mixed-mode stress intensity factors and the energy release rate under the given mechanical loading conditions. The use of this dual approach methodology allowed the verifications of both methods leading to a highly accurate numerical predictive capability to assess the effects of material orthotropy and nonhomogeneity constants on the crack tip parameters. In the case of thermal loading, the response of periodic cracks in an orthotropic FGM layer subjected to transient thermal stresses is examined by means of the developed enriched finite element method. The results presented for the thermally loaded layer illustrate the influences of the material property gradation profiles and crack periodicity on the transient fracture mechanics parameters.

Keywords: Orthotropic functionally graded materials (FGMs); Singular integral equations; Enriched finite elements; Mixed-mode stress intensity factors; Thermal stresses

1. Introduction

Functionally graded materials (FGMs) are multiphase composites that possess continuous spatial variations in the volume fractions of their constituents. These variations lead to the formation of a nonhomogeneous macro-structure with continuously varying thermomechanical properties. Ceramic/metal FGMs are originally proposed to be used as heat resistant coatings in aerospace applications (Niino and Maeda, 1990). In recent years, the feasibility of using FGMs has been explored within the contexts of a number of other technological applications such as cutting tools (Xing et al., 1998), solid oxide fuel cells (Liu et al.,

* Corresponding author. Tel.: +90 312 210 2580; fax: +90 312 210 2536.
E-mail address: sdag@metu.edu.tr (S. Dag).

0020-7683/$ - see front matter
doi:10.1016/j.ijsolstr.2007.05.010

2004), biomedical materials (Pompe et al., 2003) and piezoelectric devices (Steinhausen et al., 2004). Some of the processing methods used to deposit homogeneous ceramic or FGM coatings are known to result in a highly anisotropic structure with reduced thermomechanical properties. For example, plasma sprayed coatings have a lamellar microstructure with weak cleavage planes parallel to the boundary (Sampath et al., 1995; Sevostianov and Kachanov, 2001). Coatings processed by the electron beam physical vapor deposition technique on the other hand have a columnar structure with weak cleavage planes perpendicular the free surface (Kaysser and Ilschner, 1995; Schulz and Schmücker, 2000).

In order to take the oriented structure of FGMs into account in fracture mechanics analyses, these materials are generally modeled as orthotropic with principal directions parallel and perpendicular to the boundaries. Both analytical and computational methods are developed to examine crack problems in orthotropic FGMs. Ozturk and Erdogan (1997, 1999) considered mode I and mixed-mode crack problems for an infinite graded orthotropic medium using the method of singular integral equations. Gu and Asaro (1997) developed an analytical solution to evaluate mixed-mode stress intensity factors (SIFs) and phase angles for a graded orthotropic four point bend specimen. Guo et al. (2004) detailed an analytical procedure to calculate mode I stress intensity factors for internal and edge cracks in an orthotropic functionally graded strip. Chen et al. (2002) and Guo et al. (2005) computed dynamic stress intensity factors for orthotropic FGM layers using the approach of singular integral equations. Among the computational methods developed to study fracture mechanics of orthotropic functionally graded materials, we can mention modified crack closure method (Kim and Paulino, 2002a), mixed-mode J-integral (Kim and Paulino, 2003a), interaction integral (Kim and Paulino, 2003b), continuum shape sensitivity method (Rao and Rahman, 2005) and equivalent domain integral (Dag, 2006). Dag et al. (2004) and Chen (2005) used both singular integral equation based and computational techniques for the evaluation of mixed-mode stress intensity factors in orthotropic FGMs.

The present study aims at investigating crack problems in orthotropic functionally graded materials that are loaded by means of either crack surface tractions (mechanical loading) or temperature gradients (thermal loading). Both of the cases of mechanical loading and thermal loading are therefore within the scope of the present study. There are two major problems tackled in this paper. In the first problem, we consider an embedded crack in an orthotropic FGM layer that is subjected to mechanical loading. In the second problem, a cracked orthotropic FGM layer subjected to thermal loading is considered. The mechanical loading problem is solved by using two completely different techniques. One of these techniques is analytical and based on singular integral equations. The other one is numerical and based on the enriched finite element approach. The thermal loading problem is solved by using a single technique, that is the enriched finite element method. Hence, the present study focuses on both analytical and numerical methods in the solutions of crack problems in orthotropic FGMs.

The analytical solution procedure developed for a cracked orthotropic FGM layer subjected to mechanical loading is described in Section 2. In the development of the solution, the layer is assumed to have a lamellar structure with weak cleavage planes parallel to the boundary. Therefore, the crack in the layer is assumed to be aligned parallel to the boundary in the direction of one of the principal axes of orthotropy. Direction of material property gradation is taken as perpendicular to the crack plane. The layer is loaded mechanically through arbitrary normal and shear tractions applied to crack surfaces. Furthermore, the orthotropic FGM layer is assumed to have either free or fixed boundaries. The defined problem is reduced to a system of singular integral equations which is solved by the use of an expansion-collocation technique. In Section 3, we summarize the formulation and implementation of the enriched finite element method for mixed-mode fracture analysis of orthotropic FGMs. Enriched element technique is a general approach which can be used to solve fracture problems of orthotropic FGMs under both mechanical and thermal loading conditions.

The numerical results generated by the analytical approach and by the enriched finite elements for the mechanical loading problem described in Section 2 are presented in Section 4. Primary numerical results provided are the mixed-mode stress intensity factors and energy release rate as functions of material nonhomogeneity and orthotropy parameters. Note that the particular fracture mechanics problem examined in Section 4 has not been considered in the literature previously. This paper is the first in the literature which provides results on mixed-mode fracture parameters for an embedded crack located in an orthotropic functionally graded strip. The use of two separate ways in the solutions of the crack problems in Section 4 allowed us to carry out an in depth analysis on the accuracies of the results generated by the two methods. The main

advantage of this dual approach methodology is that it permits a direct comparison between analytical and numerical results leading to the development of a reliable numerical predictive capability. The results provided in Section 4 show that crack tip parameters computed by the numerical method are in excellent agreement with those evaluated by the analytical technique. Therefore, it is concluded that analytical and numerical techniques developed in the present study lead to highly accurate results.

In Section 5, we examine behavior of periodic cracks in an orthotropic functionally graded layer that is subjected to transient thermal stresses. The thermal fracture problem described in Section 5 is solved by means of the enriched finite element method. The primary reason behind the use of only a numerical technique in the solution of the problem is that, the defined problem does not lend itself to analytical treatment as will be further elaborated upon in Section 5. In most of the work in the literature that examine fracture behavior of FGMs under thermal stresses, it is assumed that the graded medium has an isotropic structure. The only available results in the literature on thermal fracture behavior of orthotropic FGMs seem to be provided by Chen (2005) and Dag (2006). Fracture parameters provided by Chen (2005) are evaluated by the use of an interaction integral method under steady-state thermal loading conditions. Dag (2006) examines mode I crack problems in orthotropic FGMs subjected to steady-state and transient thermal stresses. The novelty of the analysis presented in Section 5 is in the fact that, fracture mechanics parameters for orthotropic FGMs are evaluated under transient mixed-mode thermal loading conditions. This paper presents for the first time in the literature, mixed-mode stress intensity factors and energy release rate for cracks in an orthotropic FGM layer that is subjected to transient thermal stresses. The presented results could be useful in examining critical or subcritical crack propagation in orthotropic FGM layers that are used in thermal cycling environments.

2. Analytical solution for a mechanically loaded embedded crack in an orthotropic FGM layer

This section provides the details of the analytical solution developed by considering a mechanically loaded embedded crack in an orthotropic FGM layer. The parallel bounding planes of the layer are assumed to be either free or fixed. Figs. 1 and 2 depict the geometries of the crack problems under consideration. Fig. 1 shows an embedded crack in an orthotropic FGM layer that has free boundaries whereas Fig. 2 shows the same crack in a layer with fixed boundaries. In both cases, the orthotropic FGM layer is assumed to have a lamellar structure with principal directions of orthotropy coinciding with x_1 and x_2 axes. The crack is assumed to be aligned parallel to the weak cleavage planes and therefore extends along x_1-axis. Material property gradation in both layers is in x_2-direction and perpendicular to the crack plane. The crack surfaces are subjected to arbitrary self-equilibrating mixed-mode mechanical loading in each case.

If the orthotropic FGM layers shown in Figs. 1 and 2 are in a state of plane stress or strain, linear elastic constitutive relations in terms of the averaged material parameters can be expressed in the following form (Krenk, 1979)

$$\begin{bmatrix} \varepsilon_{11} \\ \varepsilon_{22} \\ \varepsilon_{12} \end{bmatrix} = \frac{1}{E} \begin{bmatrix} \delta^{-2} & -v & 0 \\ -v & \delta^{2} & 0 \\ 0 & 0 & (\kappa + v) \end{bmatrix} \begin{bmatrix} \sigma_{11} \\ \sigma_{22} \\ \sigma_{12} \end{bmatrix}, \tag{1}$$

where E is effective stiffness, δ is stiffness ratio, v is effective Poisson's ratio, κ is the shear parameter, ε_{ij}, $(i,j=1,2)$ represents strain and σ_{ij}, $(i,j=1,2)$ denotes stress. The expressions of the averaged parameters in

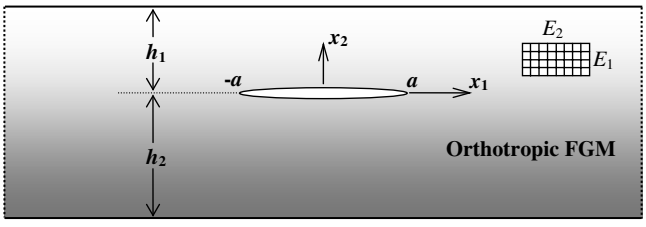

Fig. 1. An embedded crack in an orthotropic FGM layer with free boundaries.

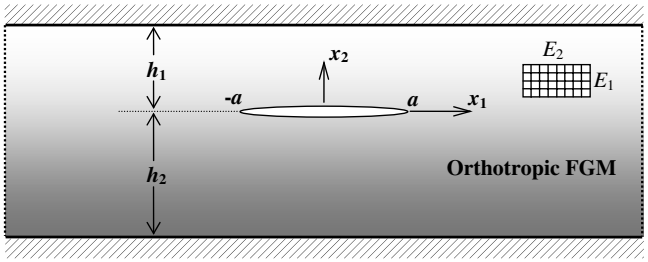

Fig. 2. An embedded crack in an orthotropic FGM layer with fixed boundaries.

terms of the engineering constants are provided in Appendix A. Note that in general all the material parameters could be functions of the spatial coordinates x_1 and x_2 in a functionally graded medium. By using suitable transformations for the coordinates and displacement and stress components, it is possible to eliminate δ from the constitutive relations. These transformations are given as

$$x = x_1/\sqrt{\delta}, \quad y = x_2\sqrt{\delta}, \tag{2a}$$

$$u(x,y) = u_1(x_1,x_2)\sqrt{\delta}, \quad v(x,y) = u_2(x_1,x_2)/\sqrt{\delta}, \tag{2b}$$

$$\sigma_{xx}(x,y) = \sigma_{11}(x_1,x_2)/\delta, \quad \sigma_{yy}(x,y) = \sigma_{22}(x_1,x_2)\delta, \quad \sigma_{xy}(x,y) = \sigma_{12}(x_1,x_2). \tag{2c}$$

where (x,y), (u,v) and $(\sigma_{xx},\sigma_{yy},\sigma_{xy})$ are the coordinates, displacements and stresses in the transformed domain, respectively. By using Eq. (2) constitutive relations in the transformed domain can now be written as follows

$$\begin{bmatrix} \varepsilon_{xx} \\ \varepsilon_{yy} \\ \varepsilon_{xy} \end{bmatrix} = \frac{1}{\hat{E}} \begin{bmatrix} 1 & -\hat{\nu} & 0 \\ -\hat{\nu} & 1 & 0 \\ 0 & 0 & (\hat{\kappa}+\hat{\nu}) \end{bmatrix} \begin{bmatrix} \sigma_{xx} \\ \sigma_{yy} \\ \sigma_{xy} \end{bmatrix}, \tag{3}$$

where $\hat{E}(x,y) = E(x_1,x_2)$, $\hat{\nu}(x,y) = \nu(x_1,x_2)$ and $\hat{\kappa}(x,y) = \kappa(x_1,x_2)$.

In order to make the defined problems analytically tractable, some simplifying assumptions are made regarding the distributions of the material properties in the orthotropic functionally graded layers. It is assumed that engineering constants E_1, E_2 and G_{12} vary in the thickness direction and that variations in these material parameters are proportional. Previous studies showed that influence of the variations in the Poisson's ratio on the SIFs is not as significant as that of the variations in the effective stiffness (Ozturk and Erdogan, 1997, 1999). Therefore, all the Poisson's ratios are assumed to be constants. These assumptions imply that ν, κ and δ are constants as well. Furthermore, variation in the effective stiffness is assumed to be represented by an exponential function. As a result, for both free and fixed layers, material properties can be expressed in the following form

$$\begin{aligned} &\nu(x_1,x_2) = \nu_0, \quad \kappa(x_1,x_2) = \kappa_0, \quad \delta(x_1,x_2) = \delta_0, \quad E(x_1,x_2) = E_0\exp(\beta x_2), \quad -\infty < x_1 < \infty, \\ &\qquad -h_2 \leqslant x_2 \leqslant h_1, \end{aligned} \tag{4}$$

where E_0 is the value of effective stiffness at $x_2 = 0$ and β is a nonhomogeneity constant. Note that ν, κ and δ are constants in both physical and transformed coordinate systems. Effective stiffness in the transformed coordinate system can be written as

$$\hat{E}(x,y) = E_0\exp(\gamma y), \qquad -\infty < x < \infty, \quad -\sqrt{\delta_0}h_2 \leqslant y \leqslant \sqrt{\delta_0}h_1, \tag{5}$$

where $\gamma = \beta/\sqrt{\delta_0}$. Governing partial differential equations can now be obtained using constitutive relations and equations of equilibrium ($\sigma_{ij,\,j} = 0$, $i, j = 1, 2$). The governing equations in the transformed coordinate system are given as follows (Sarikaya, 2005)

$$\frac{\partial^2 u}{\partial y^2}+\beta_1\frac{\partial^2 u}{\partial x^2}+\beta_2\frac{\partial^2 v}{\partial x\partial y}+\gamma\left(\frac{\partial u}{\partial y}+\frac{\partial v}{\partial x}\right)=0, \tag{6a}$$

$$\frac{\partial^2 v}{\partial x^2}+\beta_1\frac{\partial^2 v}{\partial y^2}+\beta_2\frac{\partial^2 u}{\partial x\partial y}+\beta_1\gamma\left(\frac{\partial v}{\partial y}+v_0\frac{\partial u}{\partial x}\right)=0, \tag{6b}$$

where

$$\beta_1=\frac{2(\kappa_0+v_0)}{1-v_0^2},\quad \beta_2=1+v_0\beta_1. \tag{7}$$

In the solutions of the problems depicted in Figs. 1 and 2, derivatives of the relative displacements of the crack surfaces are used as the primary unknown functions. These unknown functions are defined in the following form

$$\frac{\partial}{\partial x_1}(u_2(x_1,0^+)-u_2(x_1,0^-))=\begin{cases}f_1(x_1), & |x_1|<a\\ 0, & |x_1|>a\end{cases}, \tag{8a}$$

$$\frac{\partial}{\partial x_1}(u_1(x_1,0^+)-u_1(x_1,0^-))=\begin{cases}f_2(x_1), & |x_1|<a\\ 0, & |x_1|>a\end{cases}. \tag{8b}$$

General solutions for the displacement components are obtained by taking Fourier transforms of Eq. (6) in x-direction. For both free and fixed layers, the derived general solutions have to satisfy the corresponding boundary and continuity conditions. The conditions for the layer with free boundaries are given as

$$\sigma_{22}(x_1,h_1)=\sigma_{12}(x_1,h_1)=\sigma_{22}(x_1,-h_2)=\sigma_{12}(x_1,-h_2)=0,\quad -\infty<x_1<\infty, \tag{9a}$$

$$\sigma_{22}(x_1,0^+)=\sigma_{22}(x_1,0^-),\quad \sigma_{12}(x_1,0^+)=\sigma_{12}(x_1,0^-),\qquad -\infty<x_1<\infty. \tag{9b}$$

For the fixed layer, conditions given by Eq. (9b) are valid whereas conditions given by Eq. (9a) have to be replaced by the following set of boundary conditions

$$u_1(x_1,h_1)=u_2(x_1,h_1)=u_1(x_1,-h_2)=u_2(x_1,-h_2)=0,\quad -\infty<x_1<\infty. \tag{10}$$

The final two conditions required to be satisfied are related to the arbitrary tractions applied to the crack surfaces. For both of the layers, these conditions can be written as follows

$$\sigma_{22}(x_1,0^+)=-p(x_1),\quad \sigma_{12}(x_1,0^+)=-q(x_1),\qquad |x_1|<a, \tag{11}$$

where $p(x_1)$ and $q(x_1)$ are arbitrary self-equilibrating normal and shear tractions acting on the crack faces. The boundary and continuity conditions given by Eqs. (8)–(10) are satisfied using the general solutions derived for the displacement and stress components. Two integral equations are then derived for each of the layers considering the last two conditions given by Eq. (11). Singular terms of the integral equations are extracted by carrying out asymptotic analyses of the integrands of the related kernels. The details of the rather lengthy but straightforward procedure described above can be found in the thesis by Sarikaya (2005). For both free and fixed layers, the final form of the singular integral equations in the transformed coordinate system can be expressed in the following way

$$\int_{-a/\sqrt{\delta_0}}^{a/\sqrt{\delta_0}}\left\{\left(\frac{\lambda_1}{\pi(x-t)}+\lambda_2\mathrm{sign}(x-t)+H_{11}(x,t)\right)\phi_1(t)+\left(\frac{\lambda_3}{\pi}\ln(A_1|x-t|)+H_{12}(x,t)\right)\phi_2(t)\right\}\mathrm{d}t$$
$$=-\frac{\delta_0(1-v_0^2)}{E_0}p\left(\sqrt{\delta_0}x\right),\quad -\frac{a}{\sqrt{\delta_0}}<x<\frac{a}{\sqrt{\delta_0}}, \tag{12a}$$

$$\int_{-a/\sqrt{\delta_0}}^{a/\sqrt{\delta_0}}\left\{\left(\frac{\lambda_4}{\pi}\ln(A_2|x-t|)+H_{21}(x,t)\right)\phi_1(t)+\left(\frac{\lambda_5}{\pi(x-t)}+\lambda_6\mathrm{sign}(x-t)+H_{22}(x,t)\right)\phi_2(t)\right\}\mathrm{d}t$$
$$=-\frac{2(\kappa_0+v_0)}{E_0}q\left(\sqrt{\delta_0}x\right),\quad -\frac{a}{\sqrt{\delta_0}}<x<\frac{a}{\sqrt{\delta_0}}, \tag{12b}$$

where $\phi_1(t) = f_1(\sqrt{\delta_0}t)$, $\phi_2(t) = \delta_0 f_2(\sqrt{\delta_0}t)$, λ_i, $(i = 1,\ldots,6)$ are lengthy functions of the constants γ, κ_0 and v_0 and A_i, $(i = 1,2)$ are integration cut-off points. The expressions for λ_i, $(i = 1,\ldots,6)$ and $H_{ij}(x,t)$, $(i,j = 1,2)$ are given by Sarikaya (2005) for both of the cases of free and fixed orthotropic FGM layers. In both of the integral equations the dominant singularity is the Cauchy-type singularity, therefore the unknown functions $\phi_i(t)$ $(i = 1,2)$ possess standard square-root singularities at the end points $t = \pm\frac{a}{\sqrt{\delta_0}}$.

The integral equations given above are solved numerically using an expansion-collocation technique. In the numerical solution, first the integrals and the interval of definition are normalized using the following transformations

$$x = \frac{a}{\sqrt{\delta_0}}s, \quad |x| < \frac{a}{\sqrt{\delta_0}}, \quad |s| < 1, \tag{13a}$$

$$t = \frac{a}{\sqrt{\delta_0}}r, \quad |t| < \frac{a}{\sqrt{\delta_0}}, \quad |r| < 1. \tag{13b}$$

The unknown density functions are then expanded into infinite series in the following form

$$\phi_1\left(\frac{a}{\sqrt{\delta_0}}r\right) = \frac{1}{\sqrt{1-r^2}}\sum_{j=0}^{\infty} A_j T_j(r), \quad |r| < 1, \tag{14a}$$

$$\phi_2\left(\frac{a}{\sqrt{\delta_0}}r\right) = \frac{1}{\sqrt{1-r^2}}\sum_{j=0}^{\infty} B_j T_j(r), \quad |r| < 1, \tag{14b}$$

where $T_j(r)$ is the Chebyshev polynomial of the first kind of order j and A_j, B_j are unknown constants of the series expansions. Relative displacements of the crack surfaces have to be equal to zero at the crack tips. These conditions require that

$$\int_{-1}^{1}\phi_1\left(\frac{a}{\sqrt{\delta_0}}r\right)\mathrm{d}r = 0, \quad \int_{-1}^{1}\phi_2\left(\frac{a}{\sqrt{\delta_0}}r\right)\mathrm{d}r = 0. \tag{15}$$

Substituting from Eq. (14) into Eq. (15), it can easily be shown that $A_0 = B_0 = 0$. In order to solve the integral equations numerically, first the series expansions given by Eq. (14) are truncated at $j = N$. Truncated forms of the series are substituted into Eq. (12) and the singular terms of the integral equations are regularized using the orthogonality properties of the Chebyshev polynomials (Erdogan, 1978). Integral equations are then converted to a system of linear algebraic equations of size $2N \times 2N$ by using collocation points. Resulting equation system is solved numerically in order to compute the expansion constants A_j, B_j, $(j = 1,\ldots,N)$.

Crack tip parameters such as mixed-mode stress intensity factors and energy release rate can be determined using the computed expansion constants. Modes I and II stress intensity factors at the crack tips $x_1 = \pm a$ are defined by

$$k_1(\pm a) = \lim_{x_1 \to \pm a^{\pm}} \sqrt{\pm 2(x_1 \mp a)}(\sigma_{22}(x_1,0)), \tag{16a}$$

$$k_2(\pm a) = \lim_{x_1 \to \pm a^{\pm}} \sqrt{\pm 2(x_1 \mp a)}(\sigma_{12}(x_1,0)). \tag{16b}$$

By using the dominant parts of the stress components $\sigma_{22}(x_1,0)$ and $\sigma_{12}(x_1,0)$ near the crack tips and Eq. (14), series representations of the mixed-mode stress intensity factors are obtained as follows (Sarikaya, 2005)

$$k_1(\pm a) = \pm\frac{E_0\lambda_1}{\delta_0(1-v_0^2)}\sqrt{a}\left(\sum_{j=1}^{N} A_j(\pm 1)^j\right), \tag{17a}$$

$$k_2(\pm a) = \pm\frac{E_0\lambda_5}{2(\kappa_0+v_0)}\sqrt{a}\left(\sum_{j=1}^{N} B_j(\pm 1)^j\right). \tag{17b}$$

In an orthotropic FGM layer that has a lamellar structure, cracks generally propagate in the direction of the principal axis that is parallel to the boundary (Ozturk and Erdogan, 1999). As a result, for the problems depicted in Figs. 1 and 2, the crack is expected to propagate along x_1-axis. Therefore, energy release rate can be

calculated via the crack closure energy method by summing the work done by normal and shear stresses as the crack is closed along an infinitesimal distance da in x_1-direction. Using this approach, the expressions for the energy release rates at the crack tips are found to be in the following form (Sarikaya, 2005)

$$G(\pm a) = -\frac{\pi\delta_0(1-v_0^2)}{4E_0\lambda_1}k_1^2(\pm a) - \frac{\pi(\kappa_0+v_0)}{2E_0\delta_0\lambda_5}k_2^2(\pm a). \tag{18}$$

3. Enriched finite elements for mixed-mode fracture analysis of orthotropic FGMs

Enriched finite elements are special crack tip elements that possess the asymptotic approximations of displacement components in their displacement fields. In addition to the nodal displacements, modes I and II stress intensity factors are also considered as unknown constants in the formulation of enriched elements. Hence, using the enriched finite element approach, mixed-mode stress intensity factors can be directly calculated from the solution of a linear equation system without any post-processing. Enriched elements have been used to study various problems related to fracture of solids such as interface fracture of bonded ceramic layers (Kaya and Nied, 1993), thermal fracture of isotropic FGM thermal barrier coatings (Yildirim and Erdogan, 2004) and interface fracture of graded orthotropic coatings under mechanical loads (Dag et al., 2004). This section provides the displacement fields of enriched elements and details the finite element modeling approach followed to conduct mixed-mode fracture mechanics analyses of orthotropic FGMs.

The computational results presented in the current study are obtained by using 10-node triangular finite elements in the discretization of the orthotropic functionally graded media. Fig. 3 depicts the 10-node triangle in global and local coordinate systems. 10-node triangle possesses cubic interpolation which is particularly useful in representing smooth spatial variations in thermomechanical properties. Finite element meshes used in the computations consisted of triangular enriched, transition and regular elements. The enriched elements are located at the crack tip. Transition elements are employed in order to maintain inter-element displacement compatibility between the enriched and regular elements. In order to develop the displacement fields of enriched finite elements, we first consider a crack in an orthotropic functionally graded medium as shown in Fig. 4. x_1 and x_2 in this figure constitute a local Cartesian coordinate system whose origin is located at the crack tip. The asymptotic displacement fields at the crack tip are given by

$$u_i(x_1,x_2) = f_i(x_1,x_2)\sqrt{\pi}k_1 + g_i(x_1,x_2)\sqrt{\pi}k_2, \quad i=1,2, \tag{19}$$

where $f_i(x_1,x_2)$ and $g_i(x_1,x_2)$, $(i=1,2)$ are known functions (Kim and Paulino, 2002a; Dag et al., 2004). The geometry and displacement fields of triangular enriched, transition and regular elements can then be expressed as

$$x_1 = \sum_{j=1}^{10} N_j(r,s)(x_{1j}), \quad x_2 = \sum_{j=1}^{10} N_j(r,s)(x_{2j}), \tag{20}$$

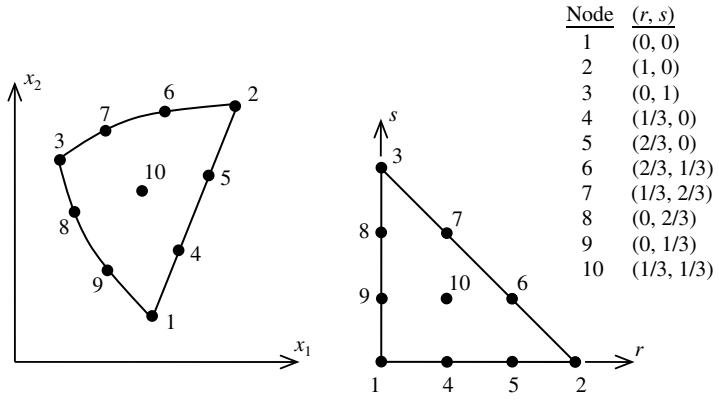

Node	(r, s)
1	(0, 0)
2	(1, 0)
3	(0, 1)
4	(1/3, 0)
5	(2/3, 0)
6	(2/3, 1/3)
7	(1/3, 2/3)
8	(0, 2/3)
9	(0, 1/3)
10	(1/3, 1/3)

Fig. 3. 10-node triangular element in global and local coordinate systems.

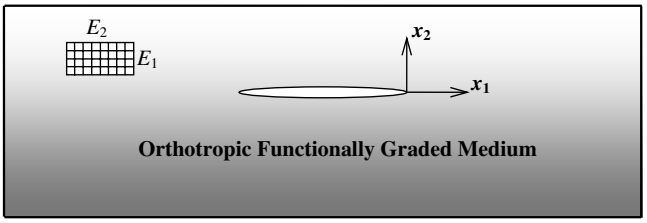

Fig. 4. A crack in an orthotropic functionally graded medium and a local coordinate system at the crack tip.

$$u_1(r,s) = \sum_{j=1}^{10} N_j(r,s)(u_{1j}) + k_1\sqrt{\pi}Z_0(r,s)\left(f_1(r,s) - \sum_{j=1}^{10} N_j(r,s)f_{1j}(r,s)\right) + k_2\sqrt{\pi}Z_0(r,s)\left(g_1(r,s) - \sum_{j=1}^{10} N_j(r,s)g_{1j}(r,s)\right), \tag{21a}$$

$$u_2(r,s) = \sum_{j=1}^{10} N_j(r,s)(u_{2j}) + k_1\sqrt{\pi}Z_0(r,s)\left(f_2(r,s) - \sum_{j=1}^{10} N_j(r,s)f_{2j}(r,s)\right) + k_2\sqrt{\pi}Z_0(r,s)\left(g_2(r,s) - \sum_{j=1}^{10} N_j(r,s)g_{2j}(r,s)\right), \tag{21b}$$

where x_{ij}, u_{ij}, $(i=1,2,\ j=1,\ldots,10)$ are nodal coordinates and displacements, respectively, $N_j(r,s)$, $(j=1,\ldots,10)$ are shape functions of the triangular element shown in Fig. 3, $f_i(r,s)$, $g_i(r,s)$, $(i=1,2)$ are asymptotic displacement functions used in Eq. (19), $f_{ij}(r,s)$, $g_{ij}(r,s)$, $(i=1,2,\ j=1,\ldots,10)$ are the asymptotic displacement functions evaluated at the nodal points and $Z_0(r,s)$ is a zeroing function. For the enriched and regular elements, this function is equal to unity and zero, respectively. As for the transition elements, the expressions for Z_0 (r,s) can be found in the paper by Dag et al. (2004).

The developed enriched finite element formulation is integrated into a fracture mechanics research finite element code FRAC2D. This program was originally developed at the General Electric Company (Kaya and Nied, 1993). Later, the fully accessible source code is extended with special graded finite elements that possess cubic interpolation in order to calculate stress and displacement fields in functionally graded materials that are subjected to mechanical or thermal loads (Dag et al., 2004; Dag, 2006). In the graded finite element approach, continuous spatial variations in the material properties are incorporated into the finite element models by computing material parameters at each Gauss point of a finite element during the formation of the element stiffness matrix. This technique is known to lead to highly accurate results (Dag et al., 2004) and is widely used to model the behavior of FGMs (Santare and Lambros, 2000; Kim and Paulino, 2002b; Dag, 2006). The cubic order graded finite elements that are used in FRAC2D are not currently available in most of the commercial finite element analysis programs.

4. Fracture mechanics parameters for a mechanically loaded embedded crack located in an orthotropic FGM layer

In this section, we present the numerical results evaluated using the analytical and computational methods by considering the embedded crack problem defined in Section 2. The two separate boundary conditions for the mechanically loaded embedded crack are depicted in Figs. 1 and 2. First, we provide some comparisons to the results available in the literature in order to verify the developed analytical and computational solution techniques. Ozturk and Erdogan (1999) calculated mixed-mode SIFs for a crack located in an infinite graded orthotropic medium using the method of singular integral equations. The problem geometry considered by Ozturk and Erdogan (1999) is similar to that shown in Fig. 1 except for the fact that h_1 and h_2 are taken as infinitely large in the analysis. Material property variation representations used by Ozturk and Erdogan (1999) are identical to those given by Eqs. (4) and (5). Some of the results provided by Ozturk and Erdogan

(1999) are generated in the present study using both analytical and finite element methods. In the analytical approach, the problem depicted in Fig. 1 is solved by taking $h_1/a = h_2/a = 20$ in order to simulate the conditions for an infinite graded orthotropic medium. Comparisons are provided by considering two separate loading conditions. In the first case, the crack is assumed to be subjected to uniform pressure over its faces ($p(x_1) = \sigma_0$, $q(x_1) = 0$) whereas the second case considers a crack subjected to uniform shear surface tractions ($p(x_1) = 0$, $q(x_1) = \tau_0$). In the finite element analyses, the infinite medium is approximated by a square plate whose side length is taken as $40a$. Note that according to Bueckner's principle, SIFs computed for a crack subjected to surface tractions are equal to those evaluated for a crack subjected to remote loads which induce the identical normal and shear stresses at the crack location in the absence of the crack. By making use of this principle, in the finite element analyses, external loads are applied at the boundaries of the plates. Only half of the plates are considered in finite element modeling by taking into account symmetry in the case of normal loading and anti-symmetry in the case of shear loading. Geometries of the plates, symmetry and anti-symmetry conditions and remote loads used in the finite element analyses are shown in Fig. 5. The comparisons of the normalized stress intensity factors are provided in Tables 1 and 2 for various values of the nondimensional nonhomogeneity parameter βa. Normalized SIFs are defined as

$$k_{1n}(a) = \frac{k_1(a)}{p_0\sqrt{a}}, \quad k_{2n}(a) = \frac{k_2(a)}{p_0\sqrt{a}}, \tag{22}$$

where $p_0 = \sigma_0$ for a crack subjected to uniform normal stress and $p_0 = \tau_0$ for a crack subjected to uniform shear. For a crack subjected to uniform normal stress, relations between the stress intensity factors calculated at the crack tips $x_1 = \pm a$ are given as

$$k_1(a) = k_1(-a), \quad k_2(a) = -k_2(-a). \tag{23}$$

In the case of a crack subjected to uniform shear, the relations are as follows

$$k_1(a) = -k_1(-a), \quad k_2(a) = k_2(-a). \tag{24}$$

Therefore, it is sufficient to tabulate the SIF values calculated at the crack tip $x_1 = a$. Deformed shapes of the finite element models and close-up views of the crack surfaces are shown in Fig. 6. By examining the results provided in Tables 1 and 2, it can be concluded that mixed-mode SIFs generated using analytical and enriched finite element methods are in excellent agreement. From Table 2, it is also observed that in the case of uniform

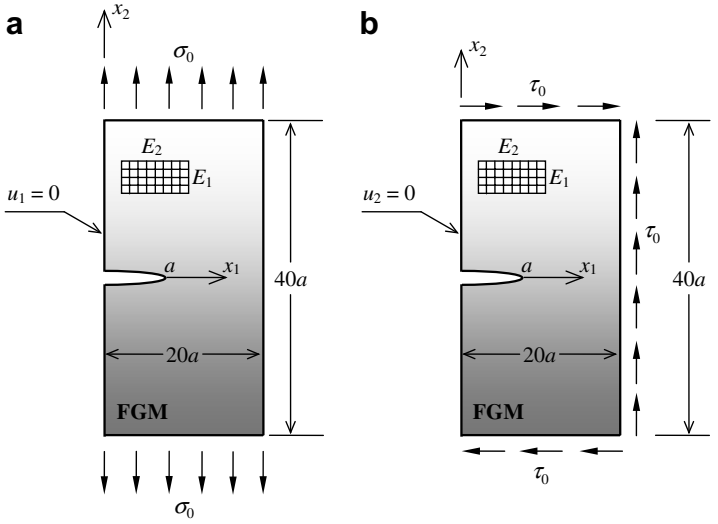

Fig. 5. Geometries and boundary conditions used in the finite element analyses of the problems posed by Ozturk and Erdogan (1999): (a) plate loaded by remote tension; (b) plate loaded by remote shear.

Table 1
Comparisons of the normalized mixed-mode stress intensity factors for a crack subjected to uniform normal stress, $p(x_1) = \sigma_0$, $q(x_1) = 0$, $\delta_0^4 = 0.25$, $\kappa_0 = 0.5$, $v_0 = 0.3$, $h_1/a = 20$, $h_2/a = 20$

βa	Ozturk and Erdogan (1999)		Analytical		Enriched elements	
	$k_{1n}(a)$	$k_{2n}(a)$	$k_{1n}(a)$	$k_{2n}(a)$	$k_{1n}(a)$	$k_{2n}(a)$
0	1.0	0.0	1.0050	0.0000	1.0064	0.0000
0.1	1.0115	0.0250	1.0135	0.0250	1.0146	0.0251
0.25	1.0489	0.0627	1.0490	0.0627	1.0496	0.0627
0.5	1.1351	0.1263	1.1351	0.1262	1.1356	0.1263
1.0	1.3494	0.2587	1.3494	0.2587	1.3498	0.2588
2.0	1.8580	0.5529	1.8578	0.5528	1.8591	0.5528

Table 2
Comparisons of the normalized mixed-mode stress intensity factors for a crack subjected to uniform shear stress, $p(x_1) = 0$, $q(x_1) = \tau_0$, $\delta_0^4 = 0.25$, $\kappa_0 = 0.5$, $v_0 = 0.3$, $h_1/a = 20$, $h_2/a = 20$

βa	Ozturk and Erdogan (1999)		Analytical		Enriched elements	
	$k_{1n}(a)$	$k_{2n}(a)$	$k_{1n}(a)$	$k_{2n}(a)$	$k_{1n}(a)$	$k_{2n}(a)$
0	0.0	1.0	0.0000	1.0036	−0.0007	1.0123
0.1	−0.0494	0.9989	−0.0494	1.0017	−0.0491	1.0043
0.25	−0.1191	0.9968	−0.1192	0.9975	−0.1197	1.0021
0.5	−0.2217	0.9965	−0.2217	0.9965	−0.2212	1.0012
1.0	−0.3862	1.0071	−0.3862	1.0071	−0.3862	1.0078
2.0	−0.5725	1.0499	−0.6249	1.0499	−0.6241	1.0505

shear loading, mode I stress intensity factor turns out to be negative at $x_1 = a$ for all considered values of βa. Hence, there is contact of crack surfaces near the crack tip $x_1 = a$ as can also be seen from Fig. 6.

The agreement between our results and those given by Ozturk and Erdogan (1999) are also seen to be excellent, except for the last case given in Table 2 for which βa is equal to 2.0 and the loading is uniform shear. In this case although the agreement between the mode II stress intensity values is again quite good, our analytical result for the mode I SIF differs from that given by Ozturk and Erdogan (1999) by an amount of 9.2%. This percent difference is evaluated by using the result given by Ozturk and Erdogan (1999) as the reference. However, as can be seen from Table 2, for this case our analytical and enriched finite element analysis results are in excellent agreement. Our computational result for the mode I SIF differs from our analytical result by an amount of only 0.13%. Therefore, it can be concluded that the result given by Ozturk and Erdogan (1999) is not as accurate as our analytical and computational results given in Table 2. In order to provide further evidence to this statement, the result for this particular case for which $\beta a = 2.0$ and the loading is uniform shear is generated using a completely different technique. Also, we provide additional comparisons to a mode I SIF result given by Rao and Rahman (2005) who considered the same problem using the continuum shape sensitivity method.

In our new analysis, the general purpose finite element analysis program ANSYS (1997) is utilized. The geometry of the problem posed by Ozturk and Erdogan (1999) is discretized by using the quadratic triangular elements available in ANSYS. Continuous variations in the material properties are incorporated into the model by specifying the material parameters at the centroid of each finite element. This approach is known to lead to highly accurate results provided that the finite element mesh is sufficiently refined (Yildirim et al., 2005b). Modes I and II stress intensity factors at the crack tip are computed by the finite elements based displacement correlation technique (DCT) which is developed by Dag et al. (2007) to study mixed-mode fracture of orthotropic FGMs. The analysis is conducted for the particular case for which there is disagreement between our results and that of Ozturk and Erdogan (1999). Table 3 shows mode I SIFs obtained in this study using the analytical approach, enriched finite elements and DCT and the results given by Ozturk and Erdogan (1999) and Rao and Rahman (2005).

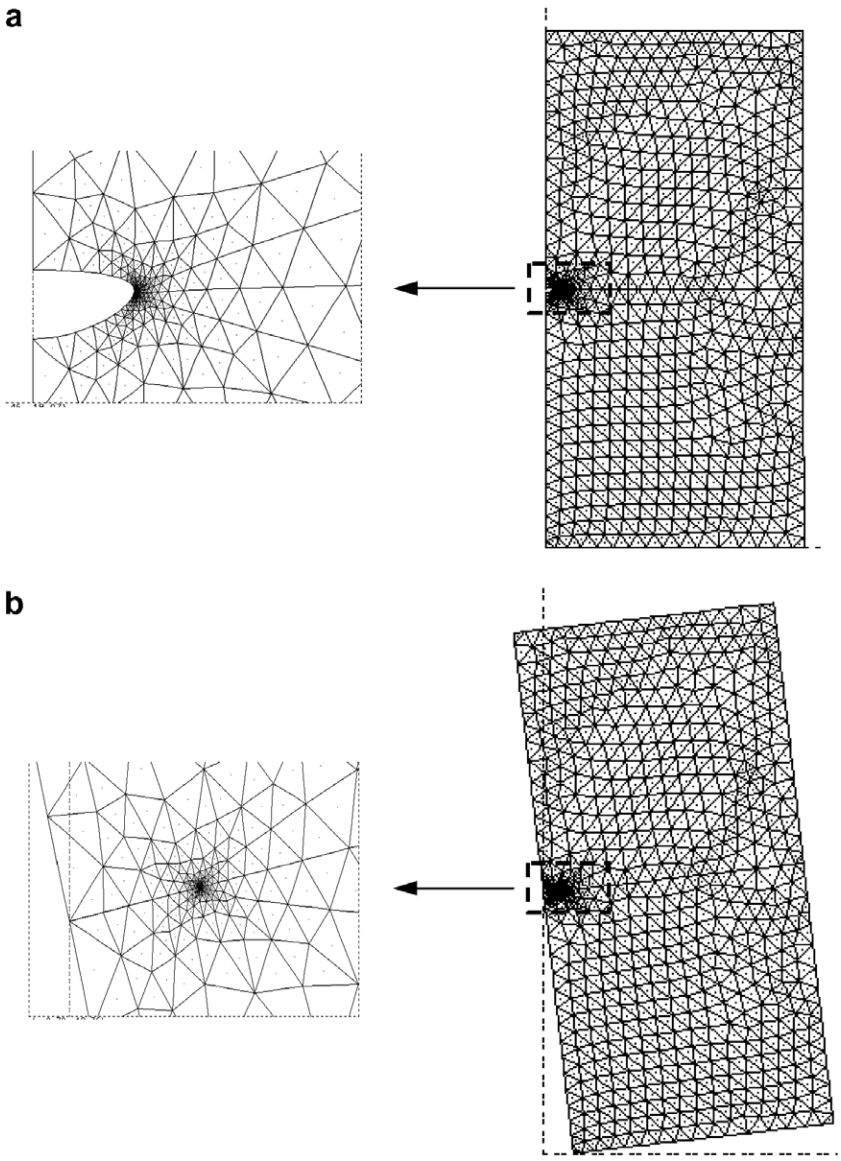

Fig. 6. Deformed shapes and close-up views of the crack surfaces: (a) plate loaded by remote tension; (b) plate loaded by remote shear.

Table 3
Comparisons of the normalized mode I SIFs obtained in the present study to those given by Rao and Rahman (2005) and Ozturk and Erdogan (1999), $p(x_1) = 0$, $q(x_1) = \tau_0$, $\delta_0^4 = 0.25$, $\kappa_0 = 0.5$, $v_0 = 0.3$, $h_1/a = 20$, $h_2/a = 20$, $\beta a = 2.0$

	$k_{1n}(a)$	Percent difference from the analytical result (%)
Present study		
Analytical	−0.6249	0.00
Enriched finite elements	−0.6241	0.13
DCT	−0.6302	0.85
Rao and Rahman (2005)	−0.6178	1.14
Ozturk and Erdogan (1999)	−0.5725	8.38

Examining the results given in the table, we observe that mode I SIF values obtained by the DCT and the analytical approach in the present study differ by an amount of 0.85% whereas the percent difference between our analytical result and the computational result given by Rao and Rahman (2005) is 1.14%. Our results and

the mode I SIF value given by Rao and Rahman (2005) are seen to be in very good agreement. Therefore, it can be concluded that the results obtained in the present study by the three different analysis techniques are more accurate than the result provided by Ozturk and Erdogan (1999).

In what follows below, we present detailed parametric analyses conducted using analytical and computational methods in order to examine the behavior of a mechanically loaded embedded crack located in an orthotropic FGM layer. Fig. 7 shows normalized modes I and II stress intensity factors versus βa and h_1/a for an embedded crack located in a layer with free boundaries (see Fig. 1). The crack is assumed to be subjected to a uniform normal stress σ_0. It is seen that magnitudes of both modes I and II stress intensity factors increase significantly as the crack gets closer to the free surface, i.e. as h_1/a is decreased from 5 to 0.1 while h_2/a is kept constant at 5. It is also observed that if the crack is located at equal distances from upper and lower boundaries ($h_1/a = 5$, $h_2/a = 5$), mode I SIF is an even and mode II SIF is an odd function of the nonhomogeneity parameter βa. This is an expected result since there is symmetry in the geometrical configuration when h_1 is equal to h_2. The results generated using the analytical approach are seen to be in excellent agreement with those obtained by enriched finite elements. Modes I and II stress intensity factors for an embedded crack located in a graded orthotropic layer with fixed boundaries (see Fig. 2) are presented in Fig. 8. The results provided in this figure show that mode II SIF is an increasing function of βa for all considered values of h_1/a whereas mode I SIF is an increasing function of βa for only smaller values of h_1/a and goes through a minimum as h_1/a becomes larger. Comparisons of the normalized energy release rates calculated considering orthotropic FGM layers with free and fixed boundaries are given in Fig. 9. Crack faces are assumed to be subjected to a uniform normal stress σ_0. Normalized energy release rate is defined as

$$G_n(a) = \frac{G(a)}{G_0}, \quad G_0 = \frac{\sigma_0^2(\pi a)}{E_0}. \tag{25}$$

Note that for an embedded crack subjected to a uniform normal traction, energy release rates at the crack tips $x_1 = \pm a$ are equal. Examining the results given in Fig. 9, it can be seen that, as the embedded crack gets closer to the bounding plane, energy release rate increases significantly for a layer with free boundaries and decreases in the case of a layer with fixed boundaries. The influence of the material nonhomogeneity parameter βa on the energy release rate is rather significant especially for the fixed orthotropic FGM layer.

The results illustrating the influence of the shear parameter κ_0 on mixed-mode SIFs and energy release rate for an embedded crack subjected to uniform pressure are provided in Figs. 10–12. In all three figures, effective Poisson's ratio of the layer is taken as 0.3. Since the sum $(\kappa_0 + \nu_0)$ has to be greater than zero, the lowest value of the shear parameter is taken as -0.25 in all three plots. Fig. 10 shows the mixed-mode SIFs versus κ_0 and h_1/a for an embedded crack located in a free layer. It is seen that the effect of the shear parameter on the stress

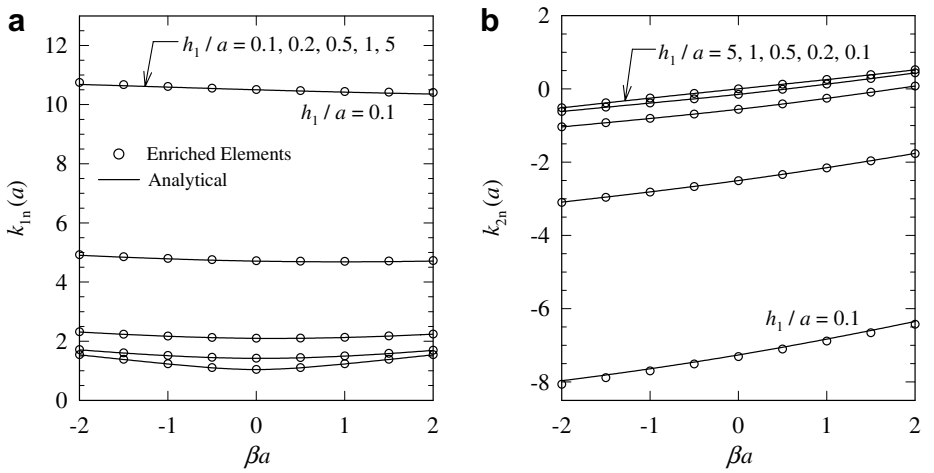

Fig. 7. Normalized mixed-mode stress intensity factors versus the nonhomogeneity parameter βa and h_1/a for the crack problem depicted in Fig. 1: (a) mode I SIFs; (b) mode II SIFs. $\kappa_0 = 2$, $\nu_0 = 0.3$, $\delta_0^4 = 2$, $h_2/a = 5$, $p(x_1) = \sigma_0$, $q(x_1) = 0$.

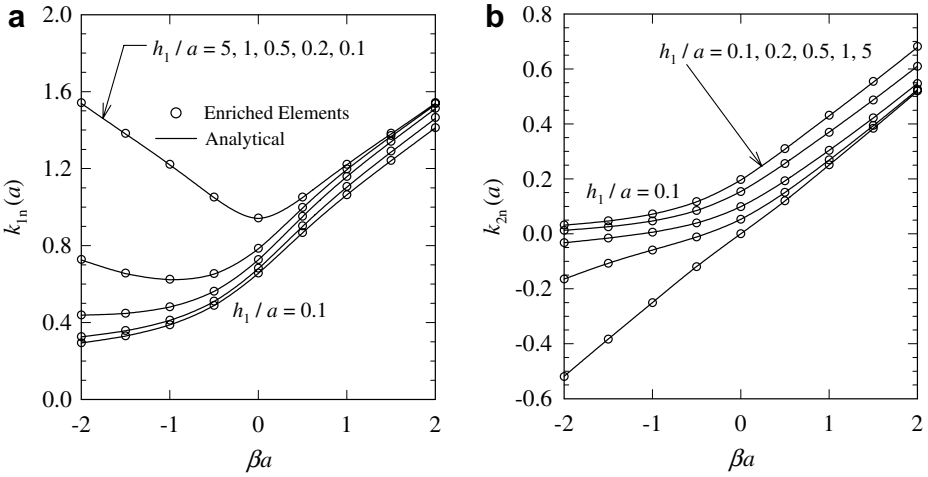

Fig. 8. Normalized mixed-mode stress intensity factors versus the nonhomogeneity parameter βa and h_1/a for the crack problem depicted in Fig. 2: (a) mode I SIFs; (b) mode II SIFs. $\kappa_0 = 2$, $\nu_0 = 0.3$, $\delta_0^4 = 2$, $h_2/a = 5$, $p(x_1) = \sigma_0$, $q(x_1) = 0$.

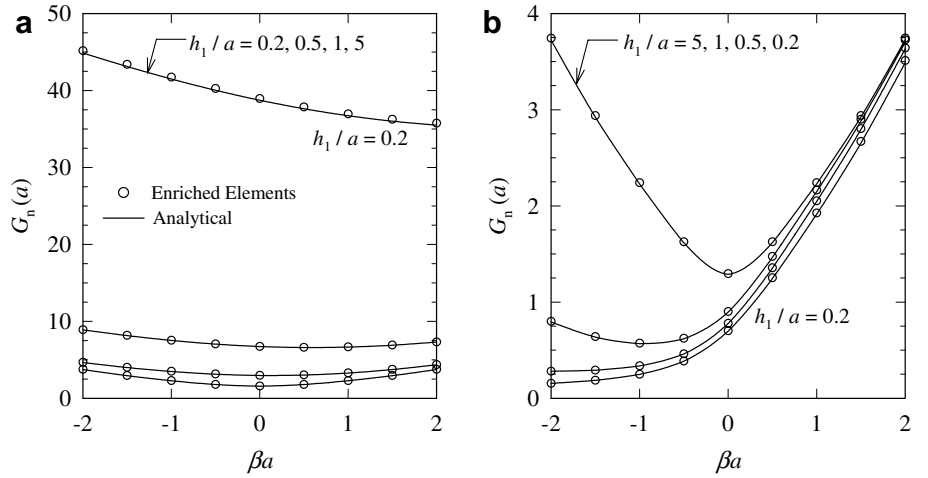

Fig. 9. Normalized energy release rates versus the nonhomogeneity parameter βa and h_1/a: (a) free layer (see Fig. 1); (b) fixed layer (see Fig. 2). $\kappa_0 = 2$, $\nu_0 = 0.3$, $\delta_0^4 = 2$, $h_2/a = 5$, $p(x_1) = \sigma_0$, $q(x_1) = 0$.

intensity factors is more pronounced when the crack is closer to the free surface. Variations of the SIFs with respect to κ_0 and h_1/a for a fixed layer are shown in Fig. 11. In this case, mode I SIF is seen to be an increasing function of κ_0 for all considered values of h_1/a. Mode II SIF on the other hand, is a decreasing function of κ_0 for small values of h_1/a and becomes almost insensitive to the variations in κ_0 as h_1/a gets larger. Fig. 12 shows normalized energy release rates evaluated considering free and fixed layers. For both layers, normalized energy release rate is found to be an increasing function of the shear parameter.

The problem of the mechanically loaded embedded crack in an orthotropic functionally graded layer is examined in this section by using both analytical and computational methods. The advantage of this dual approach methodology is that it permits a direct comparison between analytical and computational results leading to the development of a reliable numerical predictive capability. In all cases examined in this section, agreement between the analytical and computational results is seen to be quite good. Therefore, the developed enriched finite element technique of computing mixed-mode SIFs and energy release rate is concluded to be a robust way of carrying out mixed-mode fracture mechanics analysis of orthotropic functionally graded materials. The results given in Figs. 7–12 also provide highly useful insight into the fracture behavior of orthotropic

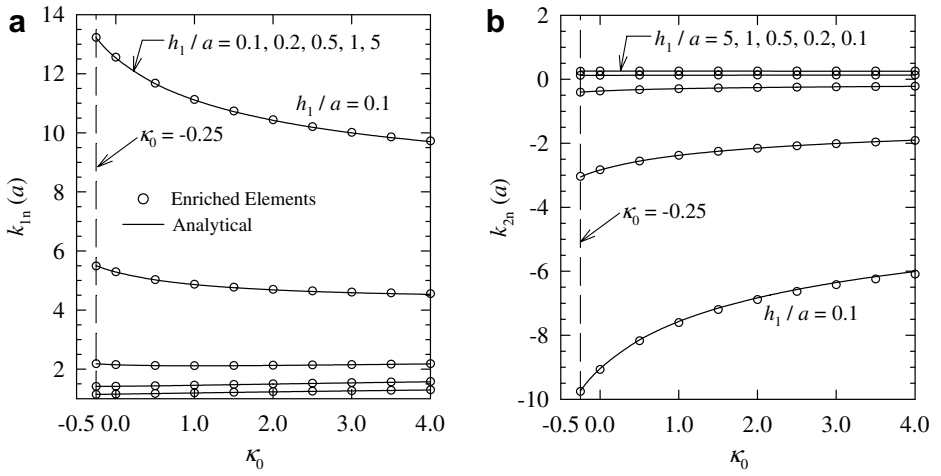

Fig. 10. Normalized mixed-mode stress intensity factors versus the shear parameter κ_0 and h_1/a for the crack problem depicted in Fig. 1: (a) mode I SIFs; (b) mode II SIFs. $\beta a = 1$, $v_0 = 0.3$, $\delta_0^4 = 2$, $h_2/a = 5$, $p(x_1) = \sigma_0$, $q(x_1) = 0$.

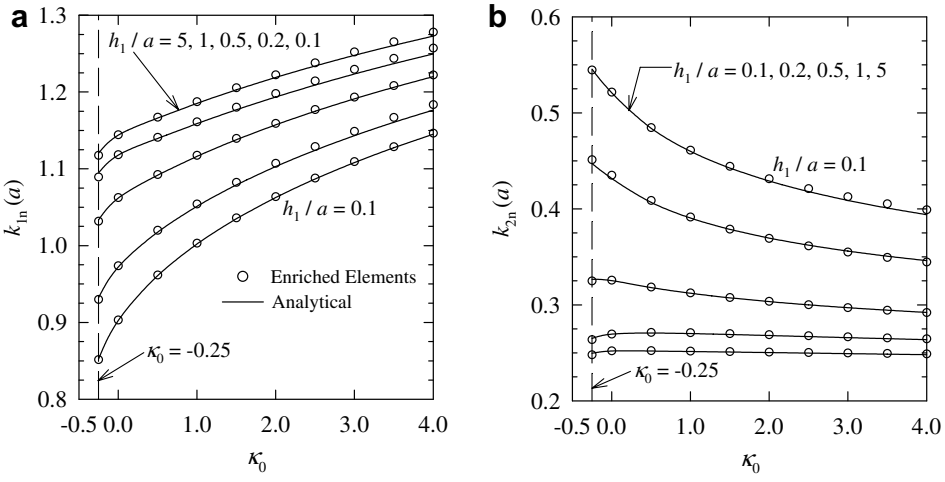

Fig. 11. Normalized mixed-mode stress intensity factors versus the shear parameter κ_0 and h_1/a for the crack problem depicted in Fig. 2: (a) mode I SIFs; (b) mode II SIFs. $\beta a = 1$, $v_0 = 0.3$, $\delta_0^4 = 2$, $h_2/a = 5$, $p(x_1) = \sigma_0$, $q(x_1) = 0$.

FGMs under mechanical loading conditions. These figures illustrate clearly the competing effects of crack geometry, material nonhomogeneity, orthotropy and boundary conditions on the crack tip parameters. The comparisons provided in this Section lead to the conclusion that the results are highly accurate and can be used as benchmarks for further investigations on fracture of orthotropic FGMs. More importantly, the given results improve our understanding of the fracture phenomenon in graded orthotropic solids subjected to mechanical loads.

In this section, we examined mixed-mode fracture behavior of an orthotropic FGM layer that has a lamellar structure. As a result, the analytical solution is based upon the assumption that the embedded crack is aligned parallel to the weak cleavage planes and perpendicular to the direction of the material property gradation. The analytical solution of the problem of a crack arbitrarily oriented with respect to the principal directions of orthotropy requires a new formulation for the derivation of the singular integral equations. This new solution can be considered as an extension of the analytical solution developed in the present study. The enriched finite element method is more general and it can be applied to the case of a crack arbitrarily oriented in a graded orthotropic medium. The implementation of the enriched finite element method for arbitrarily

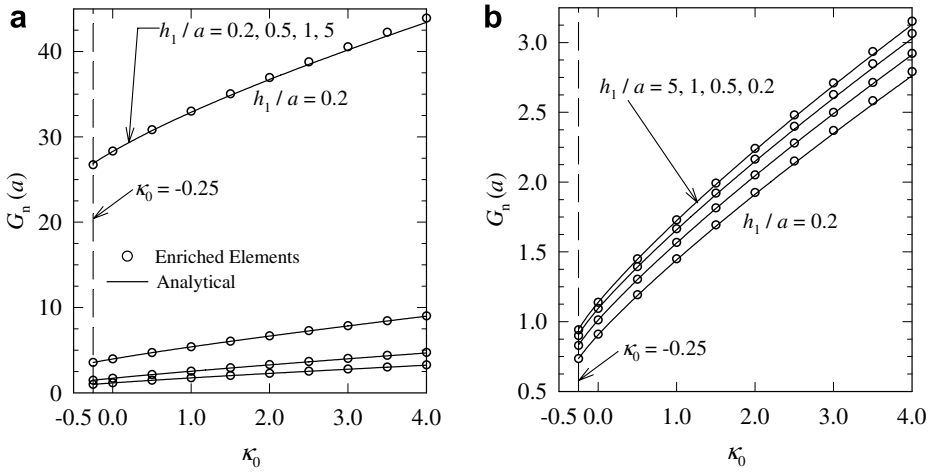

Fig. 12. Normalized energy release rates versus the shear parameter κ_0 and h_1/a: (a) free layer (see Fig. 1); (b) fixed layer (see Fig. 2). $\beta a = 1$, $\nu_0 = 0.3$, $\delta_0^4 = 2$, $h_2/a = 5$, $p(x_1) = \sigma_0$, $q(x_1) = 0$.

oriented cracks requires that the enriched elements be defined in a local coordinate system at the inclined crack tip. The mixed-mode SIFs can then be evaluated without any post-processing through the solution of a linear equation system. This analysis however is not within the scope of the present study. Computation of SIFs for arbitrarily oriented cracks in a graded orthotropic medium using enriched finite elements can also be considered as a possible extension of the work reported in this paper.

5. Periodic embedded cracks in an orthotropic FGM layer under transient thermal loading

The method of enriched finite elements is used in this section in order to carry out a detailed analysis of the thermoelastic response of periodic embedded cracks located in an orthotropic FGM layer which is subjected to thermal shock heating. Note that most of the published results in the literature on thermal fracture behavior of FGMs are generated by assuming that the graded medium has an isotropic structure. The only available results regarding the thermal fracture parameters of orthotropic FGMs seem to be provided by Chen (2005) and Dag (2006). The analysis reported in this section is an extension to both of these studies in the sense that mixed-mode fracture behavior of orthotropic FGMs is examined under transient thermal loading conditions. The enriched finite element analysis results presented here illustrate the influences of crack periodicity and material property variation profiles on the mixed-mode SIFs and the energy release rate for cracks that are located in a graded orthotropic layer.

Fig. 13 depicts the geometry of the considered problem and thermal boundary conditions. The functionally graded layer is assumed to be 100% nickel (Ni) and isotropic at $x_2 = -h_2$ and 100% alumina (Al_2O_3) and orthotropic at $x_2 = h_1$. As a result, there are smooth spatial variations in all of the thermomechanical properties from isotropy at $x_2 = -h_2$ to orthotropy at $x_2 = h_1$. Layer structure is assumed to be of lamellar type with principal directions of orthotropy coinciding with x_1 and x_2 axes. The layer contains periodic cracks of length $2a$ and spacing W and is infinitely long in x_1-direction. The cracks are aligned parallel to the weak cleavage planes and therefore they extend in the direction of x_1-axis. The depth of the layer is assumed to be sufficiently larger than the in-plane dimensions. Hence, crack tip parameters are evaluated by considering a deformation state of plane strain. Initially, the medium is assumed to be at a reference temperature of T_0 for which all the stress components are equal to zero. Afterwards, temperature of the surface at $x_2 = h_1$ is increased to $2T_0$ and that of the surface at $x_2 = -h_2$ is kept at T_0. These thermal boundary conditions imply that the layer is subjected to a thermal shock when the time is equal to zero. As a result, there will be temporal dependences for all the field quantities. The end planes perpendicular to the x_3 - direction are assumed to be insulated. Heat flow in the medium is therefore two-dimensional and temperature field is a function of x_1 and x_2 coordinates and time.

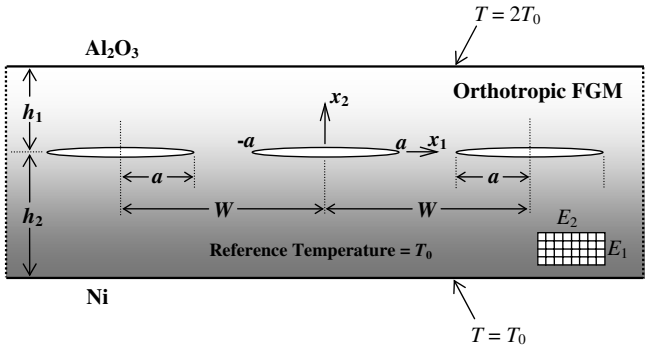

Fig. 13. Periodic embedded cracks in an orthotropic FGM layer and thermal boundary conditions.

Finite element solution of the described mixed-mode crack problem is obtained in two steps. First, transient temperature field in the orthotropic functionally graded layer is computed using a finite elements based heat transfer analysis research code HEAT2D. This research code is developed for the specific purpose of evaluating temperature fields in isotropic or orthotropic FGMs under steady-state or transient heat conduction conditions (Yildirim et al., 2005a; Dag, 2006; Yildirim, 2006). Cubic order graded finite elements are used in HEAT2D in order to evaluate temperature distribution profiles in FGMs within a high degree of accuracy. Governing partial differential equation for two-dimensional heat conduction in a graded orthotropic medium can be expressed as

$$\frac{\partial}{\partial x_1}\left(k_1\frac{\partial T}{\partial x_1}\right)+\frac{\partial}{\partial x_2}\left(k_2\frac{\partial T}{\partial x_2}\right)=\rho c\frac{\partial T}{\partial t}, \tag{26}$$

where T is temperature, k_1 and k_2 are principal thermal conductivities in x_1 and x_2 directions, respectively, ρ is density, c is specific heat and t denotes time. Computed temperature fields are then transferred to the finite elements based fracture mechanics research code FRAC2D so as to evaluate displacement, strain and stress components and to determine the crack tip parameters. Coupling between the thermal and mechanical problems is assumed to be only through the temperature field and inertia effects are neglected. Mixed-mode stress intensity factors are evaluated by means of the enriched finite element technique. In both thermal and mechanical analyses, identical finite element meshes that are composed of triangular elements are utilized. In the solution of the periodic cracking problem, engineering constants of plane orthotropic thermoelasticity are used. For a state of plane strain, the constitutive relations in terms of the engineering constants are given as follows:

$$\begin{bmatrix}\varepsilon_{11}\\ \varepsilon_{22}\\ 2\varepsilon_{12}\end{bmatrix}=\begin{bmatrix}(1-\nu_{31}\nu_{13})/E_1 & -(\nu_{12}+\nu_{13}\nu_{32})/E_1 & 0\\ -(\nu_{21}+\nu_{23}\nu_{31})/E_2 & (1-\nu_{23}\nu_{32})/E_2 & 0\\ 0 & 0 & 1/G_{12}\end{bmatrix}\begin{bmatrix}\sigma_{11}\\ \sigma_{22}\\ \sigma_{12}\end{bmatrix}+\begin{bmatrix}(\nu_{31}\alpha_3+\alpha_1)\Delta T\\ (\nu_{32}\alpha_3+\alpha_2)\Delta T\\ 0\end{bmatrix}, \tag{27}$$

where ε_{ij}, $(i,j=1,2)$ are total strain components, E_i, G_{ij}, $(i,j=1,2)$ and ν_{ij}, $(i,j=1,2,3)$ are engineering constants of plane orthotropic elasticity, α_1, α_2 and α_3 are thermal expansion coefficients in principal directions x_1, x_2 and x_3, respectively and ΔT denotes the temperature change from the reference temperature T_0. Engineering constants of orthotropic materials are related as

$$\frac{\nu_{12}}{E_1}=\frac{\nu_{21}}{E_2},\quad \frac{\nu_{13}}{E_1}=\frac{\nu_{31}}{E_3},\quad \frac{\nu_{23}}{E_2}=\frac{\nu_{32}}{E_3}. \tag{28}$$

Power functions are used to represent the continuous spatial variations in the thermomechanical properties of the functionally graded layer. The thermomechanical parameters are expressed in the following form

$$E_1(x_2) = E_1^{cr} + (E_1^{m} - E_1^{cr})\left(\frac{h_1 - x_2}{h_1 + h_2}\right)^{\gamma_1}, \tag{29a}$$

$$E_2(x_2) = E_2^{cr} + (E_2^{m} - E_2^{cr})\left(\frac{h_1 - x_2}{h_1 + h_2}\right)^{\gamma_2}, \tag{29b}$$

$$\nu_{21}(x_2) = \nu_{21}^{cr} + (\nu_{21}^{m} - \nu_{21}^{cr})\left(\frac{h_1 - x_2}{h_1 + h_2}\right)^{\beta_{21}}, \tag{29c}$$

$$\nu_{23}(x_2) = \nu_{23}^{cr} + (\nu_{23}^{m} - \nu_{23}^{cr})\left(\frac{h_1 - x_2}{h_1 + h_2}\right)^{\beta_{23}}, \tag{29d}$$

$$\nu_{31}(x_2) = \nu_{31}^{cr} + (\nu_{31}^{m} - \nu_{31}^{cr})\left(\frac{h_1 - x_2}{h_1 + h_2}\right)^{\beta_{31}}, \tag{29e}$$

$$\nu_{32}(x_2) = \nu_{32}^{cr} + (\nu_{32}^{m} - \nu_{32}^{cr})\left(\frac{h_1 - x_2}{h_1 + h_2}\right)^{\beta_{32}}, \tag{29f}$$

$$G_{12}(x_2) = G_{12}^{cr} + (G_{12}^{m} - G_{12}^{cr})\left(\frac{h_1 - x_2}{h_1 + h_2}\right)^{\gamma_{12}}, \tag{29g}$$

$$\alpha_1(x_2) = \alpha_1^{cr} + (\alpha_1^{m} - \alpha_1^{cr})\left(\frac{h_1 - x_2}{h_1 + h_2}\right)^{\delta_1}, \tag{29h}$$

$$\alpha_2(x_2) = \alpha_2^{cr} + (\alpha_2^{m} - \alpha_2^{cr})\left(\frac{h_1 - x_2}{h_1 + h_2}\right)^{\delta_2}, \tag{29i}$$

$$\alpha_3(x_2) = \alpha_3^{cr} + (\alpha_3^{m} - \alpha_3^{cr})\left(\frac{h_1 - x_2}{h_1 + h_2}\right)^{\delta_3}, \tag{29j}$$

$$k_1(x_2) = k_1^{cr} + (k_1^{m} - k_1^{cr})\left(\frac{h_1 - x_2}{h_1 + h_2}\right)^{\omega_1}, \tag{29k}$$

$$k_2(x_2) = k_2^{cr} + (k_2^{m} - k_2^{cr})\left(\frac{h_1 - x_2}{h_1 + h_2}\right)^{\omega_2}, \tag{29l}$$

$$\rho(x_2) = \rho^{cr} + (\rho^{m} - \rho^{cr})\left(\frac{h_1 - x_2}{h_1 + h_2}\right)^{\lambda}, \tag{29m}$$

$$c(x_2) = c^{cr} + (c^{m} - c^{cr})\left(\frac{h_1 - x_2}{h_1 + h_2}\right)^{\chi}, \tag{29n}$$

where the superscripts cr and m refer to the material properties of the 100% ceramic (Al_2O_3) and 100% metal (Ni) surfaces, respectively. Remaining material properties ν_{12}, ν_{13} and E_3 can be calculated by substituting the required parameters into the equalities given by Eq. (28). The power-law type representations given by Eq. (29) are highly flexible and commonly used to model continuous spatial variations in the thermomechanical properties of FGMs (Lee and Erdogan, 1998; Shen, 2002; Inan et al., 2005; Yildirim et al., 2005b). The exponents in these equations are positive constants that can be adjusted to obtain a certain type of variation profile for the orthotropic FGM layer. For example, if an exponent is greater than unity the corresponding material property has a ceramic-rich variation profile whereas for an exponent that is less than one variation profile is metal-rich.

Material characterization of orthotropic plasma sprayed deposits is considered in various studies reported in the literature (Parthasarathi et al., 1995; Leigh and Berndt, 1999; Sevostianov and Kachanov, 2001; Sevostianov et al., 2004). Parthasarathi et al. (1995) obtained experimental data on orthotropic elastic properties of alumina coatings using ultrasound measurements. Sevostianov and Kachanov (2001) developed theoretical models in order to estimate the elastic and conductive properties of orthotropic alumina coatings. In the present study, elastic properties of the 100% alumina surface at $x_2 = h_1$ are calculated by using the experimental data given by Parthasarathi et al. (1995). Principal thermal conductivities on the other hand are determined using the theoretical model developed by Sevostianov and Kachanov (2001). No published data could be

found in the literature on orthotropic thermal expansion coefficients of plasma sprayed coatings. The nominal value for the thermal expansion coefficient of alumina is given as $\alpha = 7.5(10)^{-6}\,(^{\circ}\mathrm{C})^{-1}$ by Callister (2000). This value is used as the thickness-direction thermal expansion coefficient of the 100% alumina surface. For the other two principal directions, larger values are used in order to be able to assess the influence of orthotropy on the fracture mechanics parameters. The properties of the 100% alumina surface at $x_2 = h_1$ are then given as follows:

$$E_1^{\mathrm{cr}} = 90.43\ \mathrm{GPa}, \quad E_2^{\mathrm{cr}} = 116.36\ \mathrm{GPa}, \quad G_{12}^{\mathrm{cr}} = 38.21\ \mathrm{GPa}, \tag{30a}$$

$$v_{21}^{\mathrm{cr}} = 0.28, \quad v_{23}^{\mathrm{cr}} = 0.27, \quad v_{31}^{\mathrm{cr}} = 0.14, \quad v_{32}^{\mathrm{cr}} = 0.21, \tag{30b}$$

$$k_1^{\mathrm{cr}} = 21.25\ \mathrm{W/(m\ K)}, \quad k_2^{\mathrm{cr}} = 29.82\ \mathrm{W/(m\ K)}, \tag{30c}$$

$$\alpha_1^{\mathrm{cr}} = 8(10)^{-6}(^{\circ}\mathrm{C})^{-1}, \quad \alpha_2^{\mathrm{cr}} = 7.5(10)^{-6}(^{\circ}\mathrm{C})^{-1}, \quad \alpha_3^{\mathrm{cr}} = 9(10)^{-6}(^{\circ}\mathrm{C})^{-1}, \tag{30d}$$

$$\rho^{\mathrm{cr}} = 3980\ \mathrm{kg/m^3}, \quad c^{\mathrm{cr}} = 775\ \mathrm{J/(kg\ K)}. \tag{30e}$$

Property values of the isotropic 100% nickel surface at $x_2 = -h_2$ are determined by referring to the data provided by Callister (2000) and given below

$$E_1^{\mathrm{m}} = E_2^{\mathrm{m}} = E^{\mathrm{m}} = 204\ \mathrm{GPa}, \quad v_{21}^{\mathrm{m}} = v_{23}^{\mathrm{m}} = v_{31}^{\mathrm{m}} = v_{32}^{\mathrm{m}} = v^{\mathrm{m}} = 0.31, \tag{31a}$$

$$G_{12}^{\mathrm{m}} = E^{\mathrm{m}}/(2(1+v^{\mathrm{m}})) = 77.9\ \mathrm{GPa}, \tag{31b}$$

$$k_1^{\mathrm{m}} = k_2^{\mathrm{m}} = k^{\mathrm{m}} = 70\ \mathrm{W/(m\ K)}, \quad \alpha_1^{\mathrm{m}} = \alpha_2^{\mathrm{m}} = \alpha_3^{\mathrm{m}} = \alpha^{\mathrm{m}} = 13.3(10)^{-6}(^{\circ}\mathrm{C})^{-1}, \tag{31c}$$

$$\rho^{\mathrm{m}} = 8890\ \mathrm{kg/m^3}, \quad c^{\mathrm{m}} = 456\ \mathrm{J/(kg\ K)}. \tag{31d}$$

There are certain limitations on the Poisson's ratios of orthotropic materials. These limitations are expressed by the following inequalities (Agarwal and Broutman, 1990)

$$(1 - v_{12}v_{21}) > 0, \quad (1 - v_{13}v_{31}) > 0, \quad (1 - v_{23}v_{32}) > 0, \tag{32a}$$

$$(1 - v_{12}v_{21} - v_{13}v_{31} - v_{23}v_{32} - 2v_{12}v_{23}v_{31}) > 0. \tag{32b}$$

These inequalities have to hold at every point in the orthotropic functionally graded layer.

Due to the periodicity of the cracks shown in Fig. 13, it suffices to consider only a unit cell in finite element modeling of the graded orthotropic layer. The unit cell and thermomechanical boundary conditions are depicted in Fig. 14. Heat flux and horizontal displacement components on the line AB are fixed as zero due to symmetry about x_2-axis. Since the graded orthotropic layer is assumed to be infinitely long in x_1-direction, $x_1 = W/2$ plane is also a plane of symmetry. Therefore, as the graded layer deforms, this plane should be free to undergo rigid body translation and rotation. A rigid block is used to satisfy the conditions at $x_1 = W/2$, as shown in Fig. 14. In the finite element model, the unit cell is in contact with the rigid block at $x_1 = W/2$. At the nodes that are located on the $x_1 = W/2$ plane, horizontal displacements of the unit cell are coupled with those of the rigid block. There are no constraints on the vertical displacements of the unit cell. Hence, as the

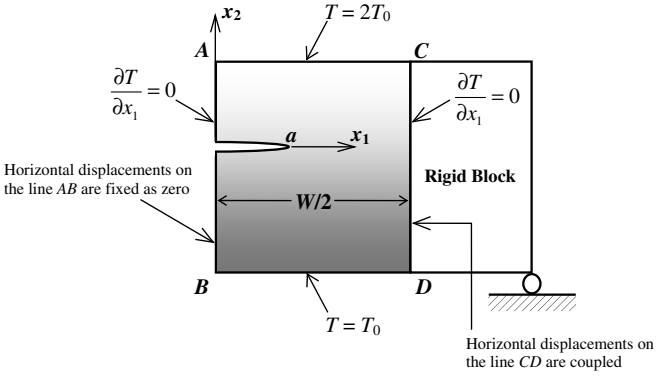

Fig. 14. Unit cell and thermomechanical boundary conditions.

graded orthotropic layer is subjected to a thermal shock at $t = 0$, $x_1 = W/2$ plane is free to undergo both rigid body translation and rotation. Due to symmetry, heat flux is set to be equal to zero at $x_1 = W/2$.

Note that the thermal fracture problem defined in this section is solved by using only a numerical technique, that is the finite element method. The primary reason of using only a numerical approach in the solution is that the defined problem can not be solved by using analytical methods based on the singular integral equations. In the analytical solutions of crack problems in orthotropic FGMs by singular integral equations, some restrictive assumptions are necessary in order to make the problem analytically tractable. For example, in the analytical solutions, the Poisson's ratios have to be taken as constants and variations in the other properties have to be taken as proportional. However, in the finite element analyses carried out in this section, none of these restrictive assumptions are used. All of the 14 material parameters of the orthotropic functionally graded layer are assumed to have independent variations governed by power functions as given by Eq. (29). A two-step analysis approach is required in the solution of the problem. First, transient temperature field in the layer has to be determined by solving Fourier's law of heat conduction which is given by Eq. (26). Then, the resulting temperature field can be provided as an input to the thermomechanical problem so as to evaluate the crack tip parameters. However, if all of the material properties are assumed to have independent variations as given by Eq. (29), it is not even possible to obtain a singular integral equation based analytical solution for the transient heat conduction problem. We also note that periodic nature of the cracking pattern introduces a further complexity into the analytical solutions of both heat conduction and thermomechanical problems. Therefore, the only way to obtain a solution to the defined problem is to use a numerical technique such as the finite element method. In what follows below, we demonstrate the application of the finite element method developed in the present study to the solution of the defined thermal fracture problem by providing numerical results. These results could be useful in the analyses of critical or subcritical crack propagation in orthotropic FGM layers that are used in thermal cycling environments such as aircraft or rocket engines.

Fig. 15 illustrates variations of normalized crack tip temperature with respect to normalized time τ for various values of relative crack spacing a/W. Normalized time is defined as

$$\tau = \frac{(\kappa)(t)}{(h_1 + h_2)^2}, \quad \kappa = \frac{k_1^{cr}}{(\rho^{cr})(c^{cr})}. \tag{33}$$

It is seen that as the upper surface is subjected to a thermal shock at $\tau = 0$, temperature of the crack tip starts increasing rapidly. The temperature subsequently approaches to a steady-state value at about $\tau = 0.6$. During the early period of transient heat conduction, temperatures evaluated for separate values of a/W are almost identical. For larger values of τ, crack tip temperature becomes a decreasing function of a/W, i.e. temperature decreases as the crack tips gets closer. Time variations of the crack tip temperature for various values of the exponent ω_2 are shown in Fig. 16. The exponent ω_2 controls the distribution profile of the thickness direction thermal conductivity k_2 [see Eq. (29l)]. For small τ values, temperature is a decreasing function of the exponent ω_2. At

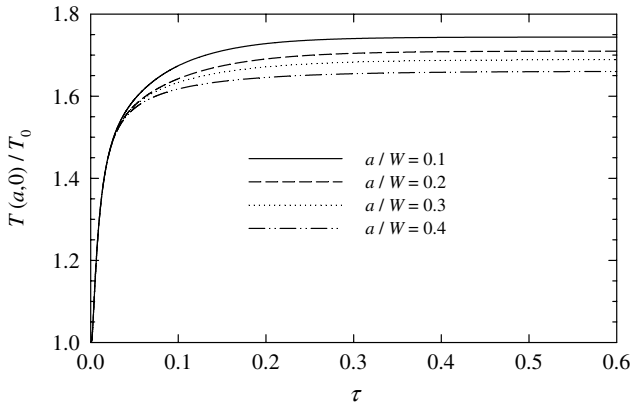

Fig. 15. Normalized crack tip temperature versus normalized time for various values of relative crack spacing a/W. $\omega_1 = \omega_2 = 2$, $\lambda = \chi = 1.5$, $h_1/W = 0.1$, $h_2/W = 0.5$.

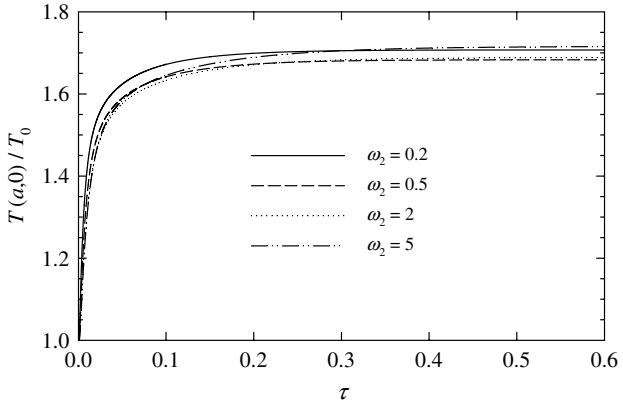

Fig. 16. Normalized crack tip temperature versus normalized time for various values of ω_2. $a/W = 0.3$, $\omega_1 = 2$, $\lambda = \chi = 1.5$, $h_1/W = 0.1$, $h_2/W = 0.5$.

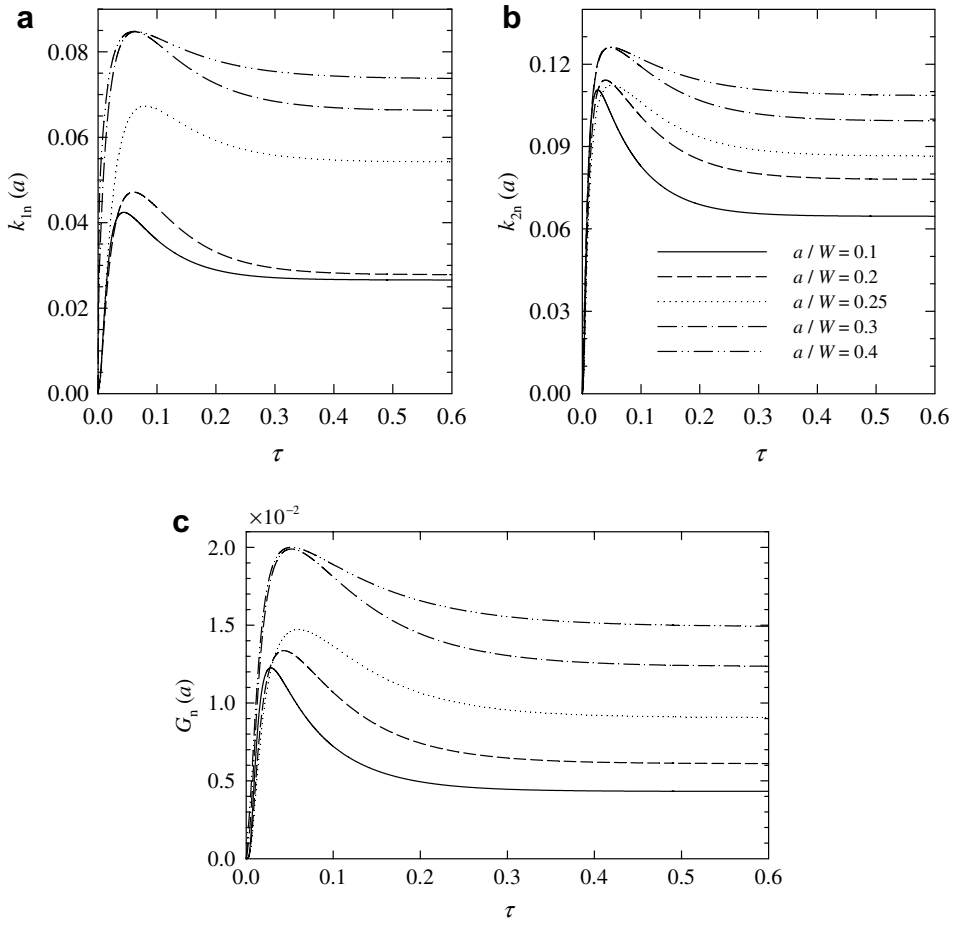

Fig. 17. Normalized crack tip parameters versus normalized time for various values of relative crack spacing a/W: (a) mode I SIFs; (b) mode II SIFs; (c) energy release rates. $\gamma_1 = \gamma_2 = \gamma_{12} = 2$, $\beta_{21} = \beta_{23} = \beta_{31} = \beta_{32} = 1.5$, $\delta_1 = \delta_2 = \delta_3 = 2$, $\omega_1 = \omega_2 = 2$, $\lambda = \chi = 1.5$, $h_1/W = 0.1$, $h_2/W = 0.5$.

steady-state, crack tip temperature goes through a minimum as ω_2 is increased from 0.2 to 5. Fig. 17 shows variations of normalized crack tip parameters with respect to normalized time for various values of relative crack spacing a/W. Normalized mixed-mode stress intensity factors and energy release rate are defined as follows

$$k_{1n}(a) = \frac{k_1(a)}{\sigma_0\sqrt{a}}, \quad k_{2n}(a) = \frac{k_2(a)}{\sigma_0\sqrt{a}}, \quad \sigma_0 = E_1^{\mathrm{cr}}\alpha_1^{\mathrm{cr}}T_0. \tag{34a}$$

$$G_n(a) = \frac{G(a)}{G_0}, \quad G_0 = \frac{(\pi a)\sigma_0^2}{E_1^{\mathrm{cr}}}. \tag{34b}$$

Due to symmetry about x_2-axis, it suffices to provide SIFs and energy release rate at the crack tip $x_1 = a$. Fracture parameters evaluated at the crack tips $x_1 = \pm a$ are related as

$$k_1(a) = k_1(-a), \quad k_2(a) = -k_2(-a), \quad G(a) = G(-a). \tag{35}$$

Examining the results given in Fig. 17, it can be seen that mixed-mode SIFs and energy release rate go through positive peaks as the graded orthotropic medium is subjected to a thermal shock. Crack tip parameters approach to their respective positive steady-state values at approximately $\tau = 0.6$. The steady-state values computed for the mixed-mode SIFs and energy release rate increase as the relative crack spacing parameter is increased from 0.1 to 0.4. Therefore, there is an amplification in the crack driving force as the crack tips get closer to each other. The amplitude of the mode II SIF is seen to be larger than that of mode I SIF which implies that sliding mode deformation prevails near the crack tip region. Deformed shape of the finite element mesh generated at $\tau = 0.05$ for a relative crack spacing of $a/W = 0.3$ is shown in Fig. 18.

Some sample results illustrating the time variations of the crack tip parameters for different values of the exponent ω_2 are provided in Fig. 19. Calculated results show that mixed-mode stress intensity factors and energy release rate are rather sensitive to the variations in the exponent ω_2. The peak and steady-state values of the crack tip parameters decrease as ω_2 is increased from 0.2 to 5. Fig. 20 illustrates the influence of the variations in the thickness direction thermal expansion coefficient α_2 on the fracture mechanics parameters. In this figure, the results are generated considering four separate values of the exponent δ_2. Note that δ_2 controls the distribution profile of α_2 [see Eq. (29i)]. Although early transient behaviors of the crack tip parameters are insensitive to the variations in the thickness direction thermal expansion coefficient, peak and steady-state values decrease as δ_2 is increased from 0.2 to 5. Hence, it can be inferred that ceramic-rich distribution profiles

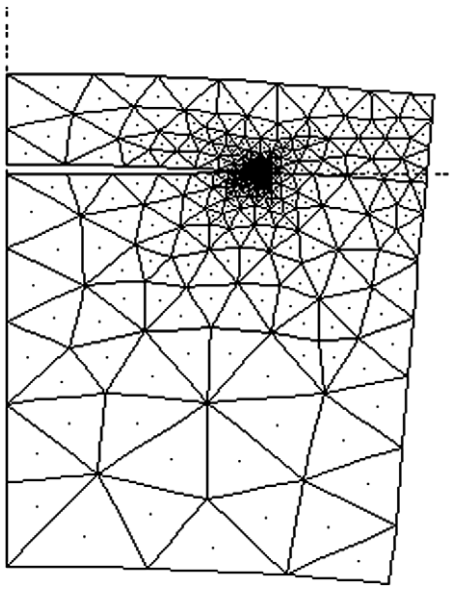

Fig. 18. Deformed shape of the finite element model of the unit cell generated at $\tau = 0.05$. $\gamma_1 = \gamma_2 = \gamma_{12} = 2$, $\beta_{21} = \beta_{23} = \beta_{31} = \beta_{32} = 1.5$, $\delta_1 = \delta_2 = \delta_3 = 2$, $\omega_1 = \omega_2 = 2$, $\lambda = \chi = 1.5$, $h_1/W = 0.1$, $h_2/W = 0.5$, $a/W = 0.3$.

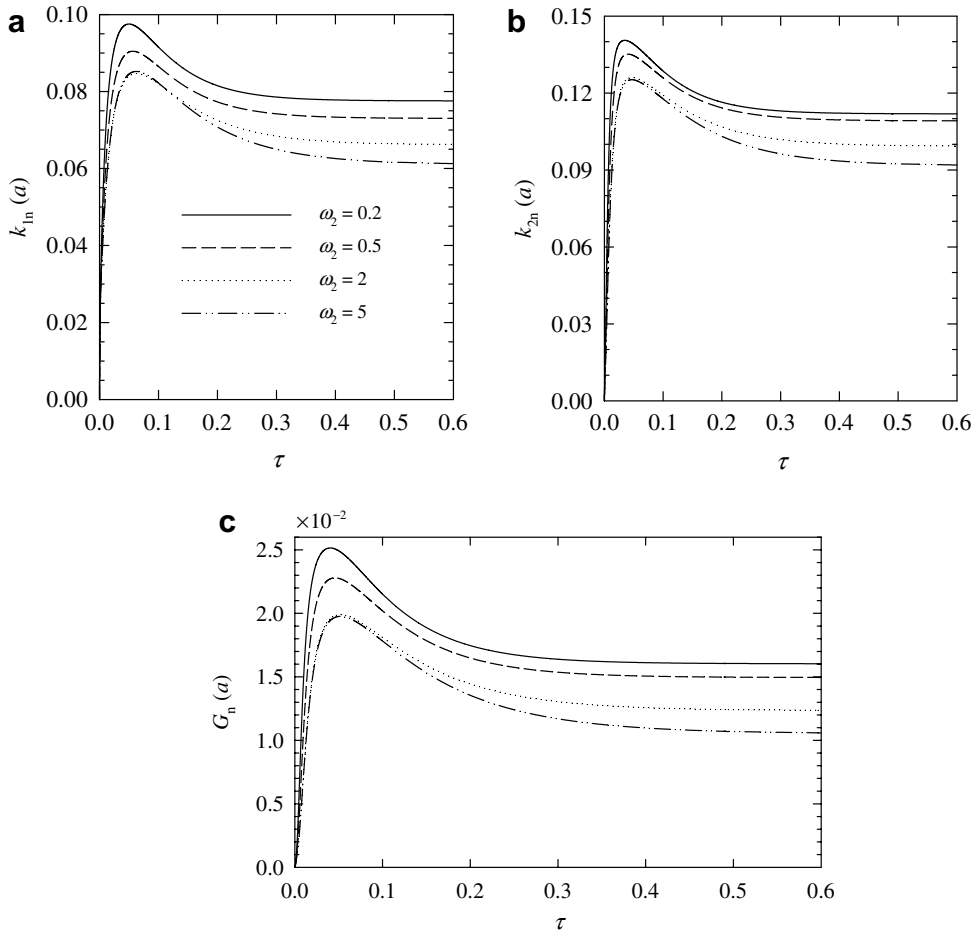

Fig. 19. Normalized crack tip parameters versus normalized time for various values of ω_2: (a) mode I SIFs; (b) mode II SIFs; (c) energy release rates. $a/W = 0.3$, $\gamma_1 = \gamma_2 = \gamma_{12} = 2$, $\beta_{21} = \beta_{23} = \beta_{31} = \beta_{32} = 1.5$, $\delta_1 = \delta_2 = \delta_3 = 2$, $\omega_1 = 2$, $\lambda = \chi = 1.5$, $h_1/W = 0.1$, $h_2/W = 0.5$.

for the material parameters k_2 and α_2 could lead to decreases in the amplitudes of both transient and steady-state crack driving forces.

6. Closure

In this study, mixed-mode fracture behavior of orthotropic functionally graded materials is examined by considering two separate loading conditions which are the mechanical and thermal types of loading. In the case of mechanical loading, an embedded crack in an orthotropic FGM layer is considered. The crack is assumed to be loaded through normal and shear tractions applied to its surfaces. Both analytical and enriched finite element methods are used to evaluate the mixed-mode stress intensity factors and energy release rate for the mechanically loaded embedded crack. Through the use of this dual approach methodology, a highly accurate numerical predictive capability is developed for the evaluation of mixed-mode fracture parameters for cracks in orthotropic FGMs that are subjected to mechanical loads. The comparisons of the mixed-mode SIFs and energy release rate computed using the enriched finite element technique to those evaluated by the analytical approach and to those available in the literature do indeed show that enriched element method is a reliable and highly accurate way of conducting mixed-mode fracture mechanics analysis of orthotropic FGMs.

Detailed parametric analyses are carried out using the analytical and computational techniques in order to examine the influences of material nonhomogeneity and orthotropy on the crack tip parameters under

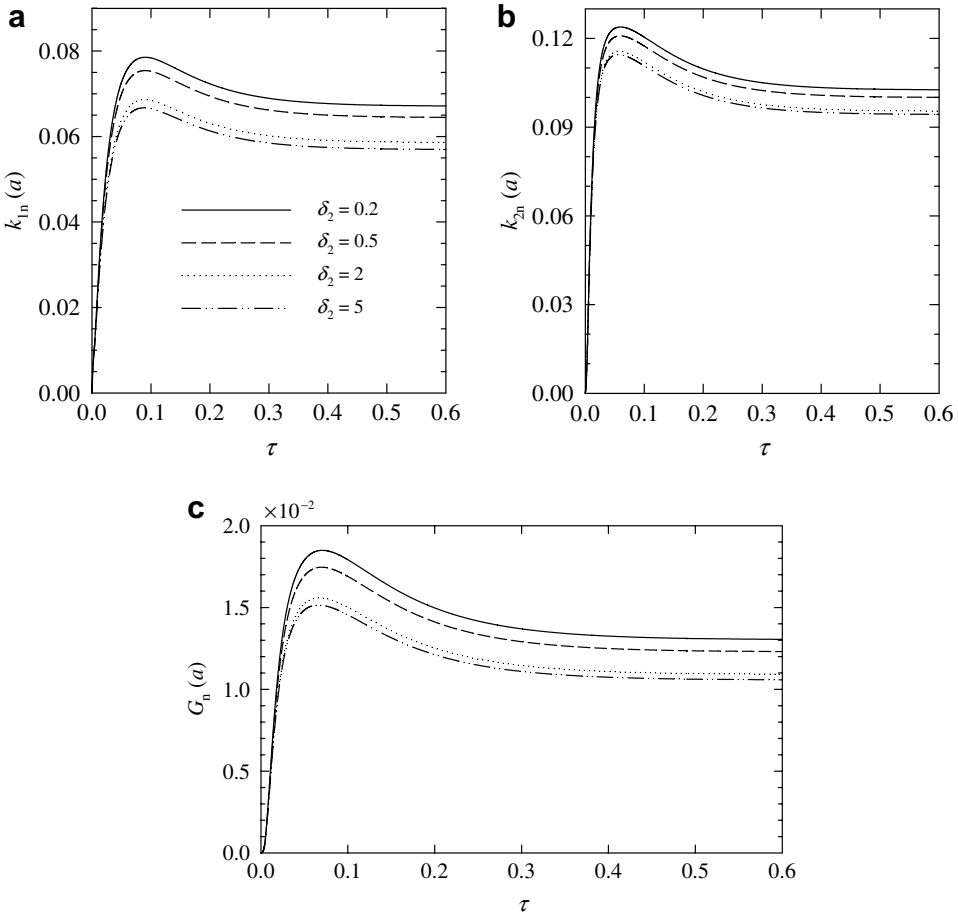

Fig. 20. Normalized crack tip parameters versus normalized time for various values of δ_2: (a) mode I SIFs; (b) mode II SIFs; (c) energy release rates. $a/W = 0.3$, $\gamma_1 = \gamma_2 = \gamma_{12} = 2$, $\beta_{21} = \beta_{23} = \beta_{31} = \beta_{32} = 1.5$, $\delta_1 = \delta_3 = 2$, $\omega_1 = \omega_2 = 2$, $\lambda = \chi = 1.5$, $h_1/W = 0.1$, $h_2/W = 0.5$.

mechanical loading conditions. The results presented in Section 4 show that for a crack located in a graded orthotropic layer and loaded by uniform normal surface tractions, energy release rate is an increasing function of the shear parameter κ_0. This trend seems to be independent of the relative location of the embedded crack in the layer and the type of the external boundary conditions. However, the nature of the influence of the material nonhomogeneity parameter βa is shown to be strongly dependent upon the relative location of the crack and the type of the external boundary conditions.

Developed enriched finite element technique is then used to solve a periodic cracking problem in an orthotropic FGM layer that is subjected to thermal loading. Temperature fields and crack tip parameters are evaluated as functions of time as the orthotropic FGM layer is subjected to a thermal shock. Mixed-mode SIFs and energy release rate are shown to go through positive peaks during the transient period of heat conduction. The peak values are found to be generally sensitive to the spatial variations of the material parameters. In particular, it is seen that ceramic-rich property distributions of the thickness direction thermal conductivity and thermal expansion coefficient could lead to reductions in the amplitudes of the energy release rates. Therefore, through the optimization of the material property variation profiles, it is possible to minimize the crack driving forces. The analytical and computational methods presented in this paper could be useful in developing algorithms for the minimization of crack driving forces in orthotropic functionally graded materials that are subjected to mechanical and thermal loads.

Acknowledgement

This work was partially supported by the Scientific and Technical Research Council of Turkey (TUBITAK) through Grant MISAG-TUN1-2004.

Appendix A. Relations between averaged and engineering constants

The constitutive relations of plane orthotropic elasticity can be expressed in terms of either averaged or engineering constants. For a state of plane stress, relationships between the averaged and engineering constants are given as follows

$$E = \sqrt{E_1 E_2}, \quad v = \sqrt{v_{12} v_{21}}, \tag{A.1}$$

$$\delta^4 = \frac{E_1}{E_2} = \frac{v_{12}}{v_{21}}, \quad \kappa = \frac{E}{2G_{12}} - v. \tag{A.2}$$

In the case of plane strain, the relationships are given by

$$E = \sqrt{\frac{E_1 E_2}{(1 - v_{13} v_{31})(1 - v_{23} v_{32})}}, \tag{A.3}$$

$$v = \sqrt{\frac{(v_{12} + v_{13} v_{32})(v_{21} + v_{23} v_{31})}{(1 - v_{13} v_{31})(1 - v_{23} v_{32})}}, \tag{A.4}$$

$$\delta^4 = \frac{1 - v_{23} v_{32}}{1 - v_{13} v_{31}} \frac{E_1}{E_2}, \quad \kappa = \frac{E}{2G_{12}} - v. \tag{A.5}$$

Note that effective Poisson's ratio and shear parameter have to satisfy the following inequalities

$$0 < v < 1, \quad \kappa > -1, \quad (\kappa + v) > 0. \tag{A.6}$$

References

Agarwal, B.D., Broutman, L.J., 1990. Analysis and Performance of Fiber Composites. John Wiley and Sons, New York.

ANSYS, 1997. ANSYS Basic Analysis Procedures Guide, Release 5.4. Canonsburg, PA, USA.

Callister, W.D., 2000. Materials Science and Engineering: An Introduction. John Wiley and Sons, New York.

Chen, J., 2005. Determination of thermal stress intensity factors for an interface crack in a graded orthotropic coating-substrate structure. International Journal of Fracture 133, 303–328.

Chen, J., Liu, Z., Zou, Z., 2002. Transient internal crack problem for a nonhomogeneous orthotropic strip (Mode I). International Journal of Engineering Science 40, 1761–1774.

Dag, S., 2006. Thermal fracture analysis of orthotropic functionally graded materials using an equivalent domain integral approach. Engineering Fracture Mechanics 73, 2802–2828.

Dag, S., Yildirim, B., Erdogan, F., 2004. Interface crack problems in graded orthotropic media: analytical and computational approaches. International Journal of Fracture 130, 471–496.

Dag, S., Ilhan, K.A., Erdogan, F., 2007. Mixed-mode stress intensity factors for an embedded crack in an orthotropic FGM coating. To appear in the Proceedings of the Multiscale and Functionally Graded Materials Conference, Oahu, HI, USA.

Erdogan, F., 1978. Mixed boundary-value problems in mechanics. In: Nemat-Nasser, S. (Ed.), Mechanics Today, vol 4. Pergamon Press, New York, pp. 1–84.

Gu, P., Asaro, R.J., 1997. Cracks in functionally graded materials. International Journal of Solids and Structures 34, 1–17.

Guo, L.-C., Wu, L.-Z., Zeng, T., Ma, L., 2004. Mode I crack problem for a functionally graded orthotropic strip. European Journal of Mechanics A/Solids 23, 219–234.

Guo, L.-C., Wu, L.-Z., Zeng, T., 2005. The dynamic response of an edge crack in a functionally graded orthotropic strip. Mechanics Research Communications 32, 385–400.

Inan, O., Dag, S., Erdogan, F., 2005. Three dimensional fracture analysis of FGM coatings. Materials Science Forum, 492–493, 373–378.

Kaya, A.C., Nied, H.F., 1993. Interface fracture analysis of bonded ceramic layers using enriched finite elements. In: Kokini, K. (Ed.), Proceedings of the Symposium on Ceramic Coatings, ASME-MD vol. 44, p. 47–71.

Kaysser, W.A., Ilschner, B., 1995. FGM research activities in Europe. MRS Bulletin 20, 22–26.

Kim, J.-H., Paulino, G.H., 2002a. Mixed-mode fracture of orthotropic functionally graded materials using finite elements and the modified crack closure method. Engineering Fracture Mechanics 69, 1557–1586.

Kim, J.-H., Paulino, G.H., 2002b. Isoparametric graded finite elements for nonhomogeneous isotropic and orthotropic materials. ASME Journal of Applied Mechanics 69, 502–514.

Kim, J.-H., Paulino, G.H., 2003a. Mixed-mode *J*-integral formulation and implementation using graded elements for fracture analysis of nonhomogeneous orthotropic materials. Mechanics of Materials 35, 107–128.

Kim, J.-H., Paulino, G.H., 2003b. The interaction integral for fracture of orthotropic functionally graded materials: evaluation of stress intensity factors. International Journal of Solids and Structures 40, 3967–4001.

Krenk, S., 1979. On the elastic constants of plane orthotropic elasticity. Journal of Composite Materials 13, 108–116.

Lee, Y.D., Erdogan, F., 1998. Interface cracking of FGM coatings under steady-state heat flow. Engineering Fracture Mechanics 59, 361–380.

Leigh, S.H., Berndt, C.C., 1999. Modelling of elastic constants of plasma spray deposits with ellipsoid-shaped voids. Acta Materialia 47, 1575–1586.

Liu, Y., Compson, C., Liu, M., 2004. Nanostructured and functionally graded cathodes for intermediate temperature solid oxide fuel cells. Journal of Power Sources 138, 194–198.

Niino, M., Maeda, S., 1990. Recent development status of functionally gradient materials. ISIJ International 30, 699–703.

Ozturk, M., Erdogan, F., 1997. Mode I crack problem in an inhomogeneous orthotropic medium. International Journal of Engineering Science 35, 869–883.

Ozturk, M., Erdogan, F., 1999. The mixed mode crack problem in an inhomogeneous orthotropic medium. International Journal of Fracture 98, 243–261.

Parthasarathi, S., Tittman, B.R., Sampath, K., Onesto, E.J., 1995. Ultrasonic characterization of elastic anisotropy in plasma sprayed alumina coatings. Journal of Thermal Spray Technology 4, 367–373.

Pompe, W., Worch, H., Epple, M., Friess, W., Gelinsky, M., Greil, P., Hempel, U., Scharnweber, D., Schulte, K., 2003. Functionally graded materials for biomedical applications. Materials Science and Engineering A 362, 40–60.

Rao, B.N., Rahman, S., 2005. A continuum shape sensitivity method for fracture analysis of orthotropic functionally graded materials. Mechanics of Materials 37, 1007–1025.

Sampath, S., Herman, H., Shimoda, N., Saito, T., 1995. Thermal spray processing of FGMs. MRS Bulletin 20, 27–31.

Santare, M.H., Lambros, J., 2000. Use of graded finite elements to model the behavior of nonhomogeneous materials. ASME Journal of Applied Mechanics 67, 819–822.

Sarikaya, D., 2005. Mixed-mode fracture analysis of orthotropic functionally graded materials, MS Thesis, Department of Mechanical Engineering, Middle East Technical University, Ankara, Turkey.

Schulz, U., Schmücker, M., 2000. Microstructure of ZrO_2 thermal barrier coatings applied by EB-PVD. Materials Science and Engineering A 276, 1–8.

Sevostianov, I., Kachanov, M., 2001. Plasma-sprayed ceramic coatings: anisotropic elastic and conductive properties in relation to the microstructure; cross-property correlations. Materials Science and Engineering A 297, 235–243.

Sevostianov, I., Kachanov, M., Ruud, J., Lorraine, P., Dubois, M., 2004. Quantitative characterization of microstructures of plasma-sprayed coatings and their conductive and elastic properties. Materials Science and Engineering A 386, 164–174.

Shen, H.S., 2002. Postbuckling analysis of axially loaded functionally graded cylindrical panels in thermal environments. International Journal of Solids and Structures 39, 5991–6010.

Steinhausen, R., Kouvatov, A., Pientschke, C., Langhammer, H.T., Seifert, W., Beige, H., Abicht, H., 2004. AC-Poling of functionally graded piezoelectric bending devices. Integrated Ferroelectrics 63, 15–20.

Xing, A., Jun, Z., Chuanzhen, H., Jianhua, Z., 1998. Development of an advanced ceramic tool material – functionally gradient cutting ceramics. Materials Science and Engineering A 248, 125–131.

Yildirim, B., 2006. An equivalent domain integral method for fracture analysis of functionally graded materials under thermal stresses. Journal of Thermal Stresses 29, 371–397.

Yildirim, B., Erdogan, F., 2004. Edge crack problems in homogeneous and functionally graded material thermal barrier coatings under uniform thermal loading. Journal of Thermal Stresses 27, 311–329.

Yildirim, B., Dag, S., Erdogan, F., 2005a. Steady state heat conduction in orthotropic functionally graded materials containing cracks: Analytical and computational techniques. In: Ziegler, F., Heuer, R., Adam, C. (Eds.), Proceedings of the Sixth International Symposium on Thermal Stresses, vol. 2, Vienna, Austria, p. 517–520.

Yildirim, B., Dag, S., Erdogan, F., 2005b. Three dimensional fracture analysis of FGM coatings under thermomechanical loading. International Journal of Fracture 132, 369–395.